LAPPEENRANTA UNIVERSITY OF TECHNOLOGY
Faculty of Technology
Degree program in Electrical Engineering

Antti Penttinen

DESIGN OF PULSED ELECTROACOUSTIC MEASUREMENT SYSTEM FOR SPACE CHARGE CHARACTERISATION

Examiners: Professor Pertti Silventoinen
D.Sc. (Tech) Xiaobing Dong

Supervisor: D.Sc. (Tech) Xiaobing Dong

ABSTRACT

Lappeenranta University of Technology
Faculty of Technology
Degree Program in Electrical Engineering

Antti Penttinen

Design of Pulsed Electroacoustic Measurement System for Space Charge Characterisation

Master's thesis

2012

63 pages, 22 figures, 10 tables, 2 appendices

Examiners: Professor Pertti Silventoinen
D.Sc. (Tech) Xiaobing Dong

Keywords: pulsed electroacoustic method, measurement system, space charge, dielectrics, pulse generator

Pulsed electroacoustic (PEA) method is a commonly used non-destructive technique for investigating space charges. It has been developed since early 1980s. These days there is continuing interest for better understanding of the influence of space charge on the reliability of solid electrical insulation under high electric field. The PEA method is widely used for space charge profiling for its robust and relatively inexpensive features.

The PEA technique relies on a voltage impulse used to temporarily disturb the space charge equilibrium in a dielectric. The acoustic wave is generated by charge movement in the sample and detected by means of a piezoelectric film. The spatial distribution of the space charge is contained within the detected signal. The principle of such a system is already well established, and several kinds of setups have been constructed for different measurement needs.

This thesis presents the design of a PEA measurement system as a systems engineering project. The operating principle and some recent developments are summarised. The steps of electrical and mechanical design of the instrument are discussed. A common procedure for measuring space charges is explained and applied to verify the functionality of the system. The measurement system is provided as an additional basic research tool for the Corporate Research Centre of ABB (China) Ltd. It can be used to characterise flat samples with thickness of 0.2–0.5 mm under DC stress. The spatial resolution of the measurement is 20 µm.

TIIVISTELMÄ

Lappeenrannan teknillinen yliopisto
Teknillinen tiedekunta
Sähkötekniikan koulutusohjelma

Antti Penttinen

Pulssitetun elektroakustisen mittausjärjestelmän suunnittelu tilavarausten ominaisuuksien tutkimiseksi

Diplomityö

2012

63 sivua, 22 kuvaa, 10 taulukkoa, 2 liitettä

Tarkastajat: Professori Pertti Silventoinen
TkT. Xiaobing Dong

Hakusanat: pulssitettu sähköakustinen menetelmä, mittausjärjestelmä, tilavaraus, sähköiset eristeet, pulssigeneraattori

Pulssitettu elektroakustinen menetelmä (PEA) on yleisesti käytetty ei-tuhoava tekniikka tilavarausten tutkimisessa. Sitä on kehitetty 1980-luvun alusta lähtien. Tilavarauksen vaikutusta kiinteän sähköeristemateriaalin luotettavuuteen voimakkaassa sähkökentässä pyritään edelleen ymmärtämään paremmin. PEA-menetelmä on laajalti käytössä tilavarausten profiloinnissa sen vakaan, yksinkertaisen ja suhteellisen halvan laitteiston ansiosta.

Menetelmä perustuu eristeessä sijaitsevan tilavarauksen tasapainotilan hetkelliseen järkyttämiseen jänniteimpulssia käyttämällä. Varausten liike synnyttää akustisen paineaallon joka havaitaan pietsosähköisellä anturilla. Havaittu signaali kertoo tilavarauksen avaruusjakauman. Mittausjärjestelmän periaate ja teoriapohja on jo pitkälti vakiintunut. Sitä hyödyntäviä sovelluksia on käytetty useissa erityyppisissä mittauksissa.

Tämä diplomityö kuvaa PEA-mittalaitteen järjestelmäsuunnittelun vaiheet. Samalla luodaan katsaus järjestelmän toimintaperiaatteeseen ja viimeisimpiin edistysaskeleisiin. Mittausjärjestelmän sähköisten ja mekaanisten osien suunnittelu ja toteutus käydään läpi vaihe vaiheelta. Laitteen toiminnallisuus varmennetaan käyttämällä yleistä mittausmenetelmää tilavarausten mittaamiseksi. Laite tulee käyttöön ABB (China) Ltd.:n Corporate Research -yksikössä perustutkimuksen apuvälineenä. Sitä voidaan käyttää 0.2–0.5 mm paksuisten levymäisten eristenäytteiden tutkimiseen DC-rasituksessa. Laitteen mittausresoluutio on 20 µm.

ACKNOWLEDGEMENTS

This master's thesis is a milestone on the path of my life that contains many markings; some of them more visible while some completely illegible to the observer looking at it. However, they all signify people without whose contribution the stone standing here wouldn't look like it does, if it were standing at all.

First, I am very grateful to my supervisor Dong Xiaobing for his guidance in the research work. His broad view and understanding of things not just technical is admirable and helped me gain a wider perspective on the research. His practical approach to work combined with highly professional and open-minded attitude left me with a lot to keep learning from.

I'm also thankful to manager Sun Huigang at CNCRC for providing me with the opportunity to work with this project and helping with all the practical arrangements to complete my research at ABB (China) Ltd.

My thanks go to the many other colleagues at CNCRC, who assisted me in solving several practical issues during the work. Especially Tian Jihuan provided invaluable help with theoretical explanations and computing problems. I appreciate their helpful and friendly attitude throughout my stay at CNCRC.

I thank Professor Pertti Silventoinen for reviewing and commenting this thesis, and also for his work at Lappeenranta University of Technology. I learned a lot about practical engineering concepts on his courses.

Finally, I want to express sincerest gratitude to my parents. They not only have laid a very solid foundation for my life, but also have always generously supported my choices in it.

Lappeenranta 21.5.2012

Antti Penttinen

TABLE OF CONTENTS

LIST OF SYMBOLS AND ABBREVIATIONS

1. INTRODUCTION 10

1.1 Background 10

1.2 Research Objectives 13

1.3 Thesis Overview 14

2. PEA MEASUREMENT SYSTEM 15

2.1 Introduction 15

2.2 Principle of the PEA System 16

2.3 Alternative PEA Systems 18

2.4 System Requirements 20

3. ELECTRICAL AND MECHANICAL DESIGN OF A PEA SYSTEM 24

3.1 Overview of the Measurement System 24

3.2 High Voltage DC Source 25

3.3 Voltage Pulse Generator 28

3.3.1 Line Type Pulse Generator 29

3.3.2 Switching Circuit 31

3.3.3 Pulse Shaping Circuit 32

3.3.4 Device Casing 35

3.4 Electrodes 35

3.5 Acoustic Signal Detector 38

3.5.1 Piezoelectric Transducer 38

3.5.2 Acoustic Impedance Matching 40

3.5.3 Detector Structure 41

3.6 Signal Acquisition System 43

4. SPACE CHARGE MEASUREMENT 44

4.1 Signal Behaviour in the System 44

4.1.1 System Calibration 45

4.2 Measurement Protocol 45
4.2.1 Reference Measurements 46
4.2.2 System Test Measurements 47
4.3 Measurement Errors 48
5. RESULTS AND DISCUSSION 50
5.1 Space Charge Formation 50
5.2 System Test Results 53
6. CONCLUSION 56
REFERENCES 58
APPENDICES
Appendix A: Control Circuit Board of the Pulse Generator
Appendix B: Photograph of the PEA System

LIST OF SYMBOLS AND ABBREVIATIONS

AC	Alternating current
BNC	Bayonet Neill–Concelman (or British Naval Connector)
BW	Bandwidth
CIGRE	International Council on Large Electric Systems
DC	Direct current
EBM	Electron Beam Method
HV	High voltage
HVDC	High voltage direct current
LIM	Laser Intensity Modulation
LIPP	Laser Induced Pressure Propagation
PEA	Pulsed electro acoustic
PET	Polyethylene terephthalate
PIPWP	Piezoelectric Induced Pressure Wave Propagation
PMMA	Polymethyl methacrylate (acrylic glass)
PTFE	Polytetrafluoroethylene
PVDF	Polyvinylidene fluoride
SMA	SubMiniature version A
TSM	Thermal Step Method
TPM	Thermal Pulse Method

b	Thickness of piezoelectric transducer
C	Capacitance [F]
C_c	Coupling capacitance
C_{dc}	Equivalent capacitance of the HV DC source
C_L	Load capacitance
C_s	Sample capacitance

c	Speed of light in vacuum [m/s]
d	Thickness of the sample
dV/dt	Slew rate
$\boldsymbol{E}$	Electric field strength [V/m]
$\boldsymbol{E}_c$	Critical electric field
$\boldsymbol{E}_{ex}$	External electric field
$\boldsymbol{E}_s$	Electric field induced by space charge
$e(t)$	Pulsed electric field
ε_0	Vacuum permittivity
ε_r	Relative permittivity
$\boldsymbol{F}$	Force [N]
f	Frequency [Hz]
f_s	Switching frequency
$h(\tau)$	Transfer function of piezoelectric transducer
η	Relative resolution
η_{eff}	Pulse efficiency
K	Propagation coefficient
L	Inductance [H]
l	Length [m]
ω	radial frequency [rad/s]
P	Power [W]
$p(t)$	Pressure signal
ρ	Charge density [C/m^3]
q	Electric charge [C]
$q(t)$	Charge signal

R	Resistance [Ω]
R_{dc}	Shielding resistance
$R(f)$	Space charge distribution function
$\hat{S}$	Peak value of output signal
$S(f)$	System response function
SNR	Signal-to-noise ratio
T	Duration of the acoustic pulse in the sample
ΔT_p	Duration of the voltage impulse
t	Time [s]
τ, $\Delta\tau$	Sampling time
U	Voltage [V]
u_b	Acoustic velocity in piezoelectric transducer [m/s]
u_{sa}	Acoustic velocity in sample
$v_{out}(t)$	Output voltage signal [V]
$v_0(t)$	Calibration voltage signal
V_{dc}	DC voltage
$v_p(t)$, V_p	Pulse voltage
$v_{sa}(t)$, V_{sa}	Voltage over the sample
Z	Impedance [Ω]
Z_0	Characteristic impedance of coaxial cable
Z_L	Load impedance
Z_b	Acoustic impedance of back electrode
Z_g	Acoustic impedance of ground electrode
Z_p	Acoustic impedance of piezoelectric transducer
σ	Surface charge [C/m^2]
σ_n	Standard deviation of noise

1. INTRODUCTION

1.1 Background

Research on the behaviour of space charges in solid electric insulating materials has gained a lot of interest during the last three decades. High electric field phenomena are becoming increasingly common in a wide range of electrical applications such as high voltage DC (HVDC) power transmission, power electronics equipment and printed circuit boards. New materials and application environments set challenges for the reliability of insulators and better understanding of the properties of dielectrics is needed. Because of their inherent nature, dielectrics are prone to accumulate trapped electrical charges within the material. These are called space charges which easily distort the original internal electric field distribution and cause extremely high local electric fields. This in turn may cause the insulating material to degrade which can lead to electrical breakdowns and electrostatic discharges [1, 2]. Even very modest charge concentrations can give rise to field distortions in range of several kV/mm or even tens of kV/mm. Even in highly refined materials used in high voltage insulators there may be sufficient amount of impurities acting as possible sources of charge traps. Space charge occurs whenever the rate of charge accumulation is different from the rate of charge removal, and may be due to electrons or ions. They arise due to both moving and trapped charges which are formed due to three processes in a dielectric under an electric field [3]:

1) The external electric field orients the dipole charges within the bulk of a homogenous material. The associated space charge is a sharp step function with two peaks at the electrodes.

2) The electric field induces ion migration where negative charges move towards the positive electrode and vice versa. The mobility of the various charge carriers are not equal resulting in random accumulation in the vicinity of electrodes. The space charge is called “heterocharges”. This type of space charge is often the result of material impurities.

3) Charges injected at the electrodes generate a space charge when the mobility is low. The charges appear in the immediate vicinity of the electrode-bulk interfaces and have the same polarity as the electrode. These charges are called “homocharges”.

Additionally, there is some evidence showing the influence of mechanical deformation on the formation of space charges [4]. Especially when operating under high electric stress these effects on component and system performance become a critical subject. The reliability of an insulator is determined by the local electric field $\boldsymbol{E}(z)$ that is a vector sum of the externally applied electrostatic field $\boldsymbol{E}_{ex}$ and the space charge field $\boldsymbol{E}_{s}$. The local field must stay below a critical field $\boldsymbol{E}_{c}$ as expressed in equation

$$\boldsymbol{E}_{\mathrm{ex}}(z) + \boldsymbol{E}_{\mathrm{s}}(z) < \boldsymbol{E}_{\mathrm{c}}. \tag{1.1}$$

Critical field, E_c, can be the electric field to cause premature ageing and deterioration of dielectric material, which finally brings to a breakdown.

To gain understanding of the material behaviour under electric stress and to have the ability to predict it as a function of time, it is necessary to observe the spatial distribution of the electric field.

Space Charge Measurement Techniques

Space charge formation in dielectrics is much studied using various thermal, acoustic and optical methods specifically developed for this purpose [5, 6]. During the 1980s, the first non-destructive techniques for direct observing the space charge distribution along the thickness of a sample were developed [7, 8]. Table 1 presents the progress in space charge investigation techniques. The pulsed electroacoustic (PEA) technique studied in this work was first proposed in Japan by Takada and Sakai in 1983 [9] and further developed into a mature technique by Takada et al. in 1987 [10].

Fields of Interest

In today's research for high electric field applications, among the topics receiving the most interest are HVDC power transmission and electronics in space environment [11, 12]. Polymer materials are used widely in electrical cable insulation and these applications set challenging operating conditions for the dielectrics, e.g. 30 years of lifetime under continuous electric and thermal stress. In space environment, the materials are continuously exposed to cosmic rays, electrons, protons and ions of varying energy levels. Low-energy charges can accumulate on surfaces potentially leading to electrostatic discharges that may cause severe malfunctions of the electrical equipment. High-energy charges can pass through the outer metal layers and accumulate into the equipment such as electric cables inside the spacecraft. To ensure safe operation of satellites, space stations etc., solid understanding of charging and discharging phenomena in space environment is needed. For this purpose, some on-

site surface and internal space charge measurement methods have been developed as introduced by Fukunaga [12].

Table 1. Research progress in space charge measurement technologies [7].

Time period	**Research topics**	**Technique remarks**
1970s	TSC (Thermally Stimulated Current) TSSP (Thermally Stimulated Surface Potential) TL (Thermoluminescence)	Destructive methods
1980s	PWP (Pressure Wave Propagation method) LIPP (Laser-Induced Pressure Pulse method) PPS (Piezoelectrically Generated Pressure Step method) PPP (Piezoelectrically Generated Pressure Pulse method) PEA (Pulsed Electroacoustic method) TSM (Thermal Step method)	Non-destructive methods
1990s	Extensive research on the characteristics of space charge distribution in dielectrics. Application in development of new insulating materials.	Application specific
2000s	Improvement and wider application of existing methods.	

In countries that are developing and urbanising with rapid pace, there is massive and growing demand for electricity. Highly efficient electrical transmission is required for effective electricity distribution over long distances. In recent years the use of HVDC power transmission has increased significantly and the trend is expected to continue. The “comeback of DC” has been largely made possible by continuous development of HVDC power transmission systems and technologies, which is also a core business for ABB. Space charge research in cable insulation is a current issue especially in HVDC Light transmission systems. In high voltage cables the polymer materials experience high electrical stress and local deformations of the electric field become a critical issue. New polymeric insulation materials are investigated and methods for testing their reliability in operating environments are being developed. Space charge profiling is one of the key techniques for investigating high voltage insulators and it is part of that on-going research in ABB’s Corporate Research Centre in Beijing.

1.2 Research Objectives

The main goal of this work is to set up a pulsed electro-acoustic measurement system as a diagnostic tool for investigating space charge profiles in polymer materials. Since the PEA method is a mature technology, the equipment has been commercially available for some time. However, the high cost of these products give motivation for inexpensive solutions applicable in basic research purposes.

The design of the PEA instrument is done by applying a systems engineering approach. This Master's thesis aims to present a comprehensive overview of the theoretical and practical issues related to the topic. In order to maintain the overall perspective, the more in-depth theoretical examination is left to the reader's own interest. Published material on research conducted using the PEA method is reviewed. Based on the available works, the theoretical principle of the method is explained. The system is calibrated and tested with dielectric samples to verify its functionality and to provide a guide on how to use the instrument for conducting measurements. The instrument is designed for measuring thin plate sample under DC fields. The desired system specifications are as follows:

- Adjustable DC bias voltage up to 10 kV
- Able to measure samples with thickness of 0.2–1 mm
- Relative resolution of the measurement ca. 5 %
- Measurement frequency 100–400 Hz
- Adjustable voltage pulse input
- Signal acquisition by digital oscilloscope
- Capability of operating the system in normal laboratory environment
- Easily portable

The secondary goal is to provide a thorough explanation of the design process of a PEA system and the many practical issues and details that are encountered should be beneficial to the ones who choose to undertake a similar project. Despite the large body of research material available, a detailed work that compiles the multitude of design problems wasn't found to be available. This work aims to fill that gap in the field.

1.3 Thesis Overview

The work is conducted at Power Technology Department, Corporate Research Centre, ABB (China) Ltd., which focuses on researching insulator materials for AC and DC power transmission systems. The project is part of the fundamental research on polymer materials conducted at ABB. The structure of the PEA system is based on previous works that utilise the method for space charge research.

Chapter 1 provides an overview on the background and development of space charge profiling methods and introduces some of the application fields receiving the most attention in today's research. Furthermore, the motivation and objectives of this work are explained.

Chapter 2 presents the PEA method and explains its operation principle. An overview of different PEA systems and their applications is provided. Here also is explained the detailed system requirements of the PEA measurement device designed in this work.

Chapter 3 contains a description of the design process of the PEA system. The electrical and mechanical design of each component of the system is explained along with the overview of the whole measurement system.

Chapter 4 describes the testing of the PEA equipment by using it to conduct space charge measurements. The measurement protocol, system calibration and signal recovery methods are explained. In addition, some reference measurements are introduced to further help verifying the functionality of the system.

Chapter 5 presents and discusses the measurement results. Space charge formation is explained with using the measurements as illustration.

Chapter 6 gives a summary of this thesis and the results achieved in the work. Suggestions for improving the system performance are provided.

2. PEA MEASUREMENT SYSTEM

2.1 Introduction

The pulsed electroacoustic method was developed as an additional tool for non-destructive study of space charges in dielectrics. Today it is one of the more widely used methods in this research field and is has been widely applied in various needs also in the industrial sector [13, 14]. The method originated in Japan as mentioned in Chapter 1 and has since gradually found interest in other countries. The PEA method is based on acoustic measurement technique together with the other commonly used pressure wave propagation (PWP) method. The PWP method is further classified into piezoelectric induced (PIPWP) and laser induced (LIPP) methods. These techniques rely on external excitation applied on the dielectric sample, causing the space charges in material bulk to be dislocated. The movements of the charged particles generate a physical response that can be detected and analysed to obtain the density, polarisation and location of the charges. Table 2 presents a comparison between the various acoustic space charge measurement techniques.

The PEA technique is currently one of the most commonly used methods for space charge profiling because it is non-destructive, meaning that repeated measurements can be easily carried out on the same sample. Advantages of the PEA technique over the other methods include the following:

- Simple and robust equipment which makes it easy to apply into various environments and industrial needs.
- Simple operation principle not requiring complex mathematical treatment.
- It allows observing dynamic phenomena.
- It is a safe method because the high voltage circuit and signal detection circuit are completely separated, preventing damage to the detection system in case of an electric breakdown.
- The detection circuit can be easily shielded electrically resulting in less noisy output signal.

Table 2. Acoustic methods for non-destructive space charge measurement.

Measurement method	Excitation method	Measurement signal
PIPWP	Pressure wave by piezoelectric device	Displacement current
LIPP	Pressure wave by pulsed laser irradiation	Displacement current
PEA	Electric pulse	Pressure signal
TSM	Thermal step	Electric current
TPM	Thermal pulse	Electric signal
LIM	Thermal pulse by laser intensity modulation	Electric current
EBM	Electron beam irradiation	Electric current

2.2 Principle of the PEA System

The principle of the PEA method is presented in Figure 1 according to the explanation provided by Takada et al. [15]. A sheet sample with thickness *d* and bulk space charge distribution $\rho(x)$ is placed between two electrodes. An external electric field impulse $e(t)$ is applied over the sample, inducing a perturbation force $\boldsymbol{F}(t)$ on the charges q according to Coulomb's law:

$$\boldsymbol{F} = q\boldsymbol{E}. \tag{2.1}$$

The force causes slight and rapid dislocation of each charge, which generates acoustic pressure waves $p(t)$. These waves are proportional to the charge distribution $\rho(x)$ in the sample. The acoustic wave $p(t)$ propagating through the sample and ground electrode are detected by a piezoelectric transducer that transforms the pressure waves into electrical signal $q(t)$. The amplitude of the output signal is proportional to the charge quantity, and delay indicates the distance of the charges from the sensor revealing the position of the charge. The space charge accumulation as a function of time and polarisation field strength can be examined by applying a DC voltage V_{dc}. This results in

introduction of surface charges $\sigma(0)$ and $\sigma(d)$ by both the DC voltage and the space charge that also generate acoustic waves during the measurement, corresponding to the thickness of the sample. The acoustic pressure wave can be expressed as a function of time:

$$p(t) = K\left[\sigma(0)e_{\mathrm{p}}(t) + u_{\mathrm{sa}}\int_0^{\infty}\rho(\tau)\,e_{\mathrm{p}}(t-\tau)d\tau + \sigma(d)e_{\mathrm{p}}\left(t-\frac{d}{u_{\mathrm{sa}}}\right)\right]. \qquad (2.2)$$

Here K is the transmission coefficient of the acoustic wave in the ground electrode-sample interface. Sampling time is τ, thickness of the sample d and the acoustic velocity in the sample is u_{sa}. The output signal of the system $v_{\mathrm{out}}(t)$ can be represented in frequency domain as the convolution of the system function $S(f)$ and the pressure wave $P(f)$:

$$V_{\mathrm{out}}(f) = S(f)P(f) = S(f)\left[\frac{\sigma(0)}{u_{\mathrm{sa}}\Delta\tau} + R(f) + \frac{\sigma(d)}{u_{\mathrm{sa}}\Delta\tau}\exp\left(-\frac{i2\pi fd}{u_{\mathrm{sa}}}\right)\right]. \qquad (2.3)$$

Here the sampling time is denoted by $\Delta\tau$. The space charge distribution $R(f)$ can be obtained if the system response $S(f)$ is known. The system response consists of the transducer and amplifier response together with the attenuation and dispersion of the acoustic wave as it propagates through the system. It is possible to remove the effect of $S(f)$ through appropriate calibration method which is explained in Chapter 4.

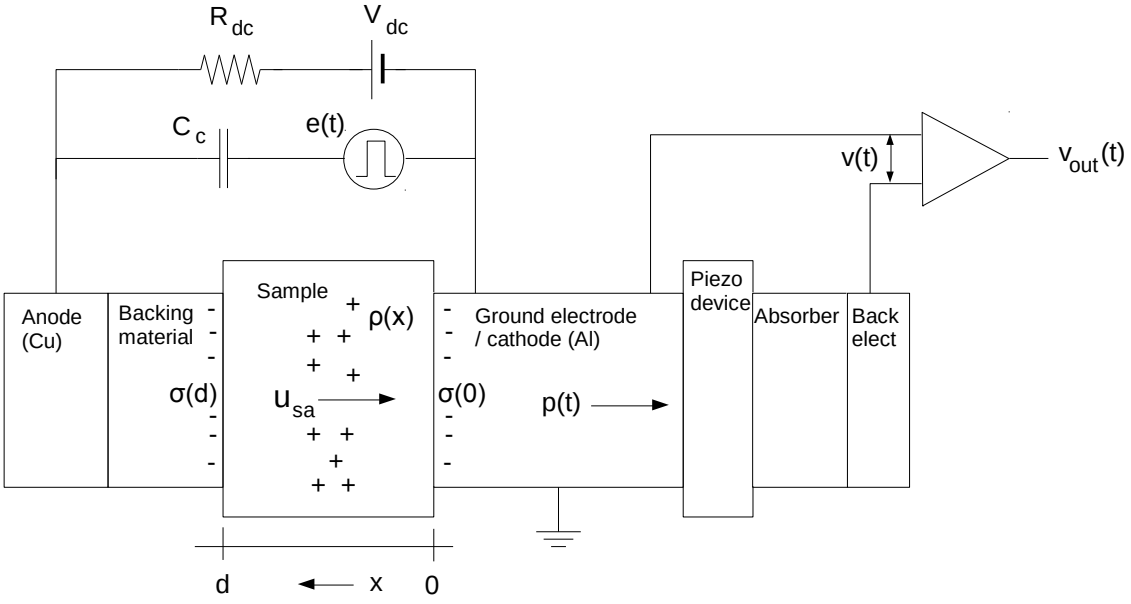

Figure 1. Schematic of the basic PEA space charge measurement system.

The method can be used to directly obtain the space charge distribution $\rho(x)$, along with the electric field distribution $E(x)$ and potential distribution $U(x)$ along the thickness of

the sample. In addition, the mobility of charges for example in photo-conductive materials can be estimated by using different calculating methods [16]. Figure 2 shows typical experimental results using the PEA method.

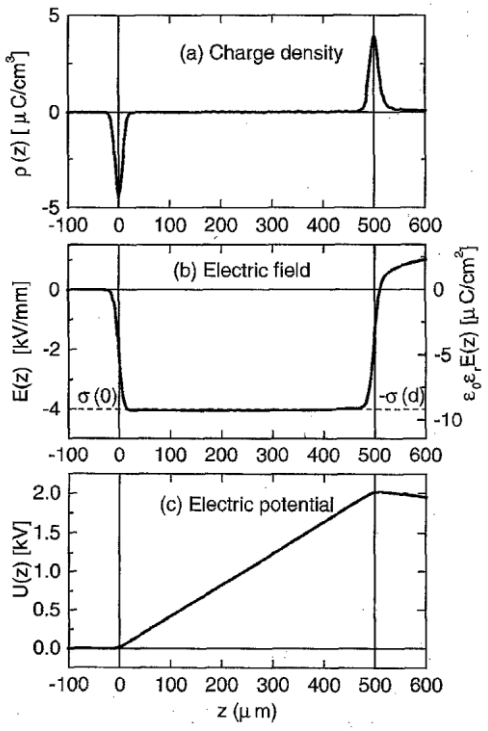

Figure 2. An example of PEA measurement results from a sample containing no space charge [15].

2.3 Alternative PEA Systems

There has been strong scientific motivation for continuous development of the PEA method. New PEA systems with unique features have been developed to meet different research needs, as introduced by Fukunaga [13]. Table 3 presents the current advancements and possible added functions of the PEA technique. High speed (high repetition rate) measurement systems enable the study of the space charge dynamics under transient electrical stress such as AC field or impulse voltage present at insulation breakdowns [17]. PEA systems with high spatial resolution for measuring thinner films [18] and high sensitivity for gaining more accurate space charge profiles [19] have been successfully built. A drawback of the conventional PEA measurement is that it can measure space charges only in two dimensions: amplitude and the spatial location along the thickness of the sample. Thus, it doesn't take into account planar non-uniformities in the surface direction of the sample. Some three-dimensional techniques such as acoustic lens method have been developed [20] to address this question. The

latest reported improvement in the lateral resolution of a 3D system is 100 µm [14]. Additional information can be gained by performing simultaneous complementary measurements while observing the space charges. A PEA system without an electrode on the sample surface can be applied for space charge observation under irradiation [21]. This is useful for measuring various materials used in space applications. Other solutions have implemented temperature control and simultaneous measurement of conduction current [22, 23], allowing the estimation of conductivity at any depth of the sample. In addition to sheet samples, also power cables can be measured using the regular PEA system with slight modifications [24]. For more practical applications such as on-site monitoring of charge accumulation, a miniature PEA electrode cell and a portable measurement system was developed [25]. The PEA method can also be applied to investigate components such as capacitors and printed circuit boards for reliability testing.

Table 3. Latest advancements of the PEA measurement system. Typically the values in resolutions and sensitivity vary depending on the application.

System property	Latest improvement/addition
Spatial resolution: Thickness direction Surface direction	 2 µm 100 µm (with 5 µm in thickness direction)
Repetition rate (time resolution)	10 µs
Sensitivity	0.03–0.15 C/m^3
Complementary measurement: Current Luminescence Thermally stimulated current Chemical analysis Electron irradiation	 Conduction, displacement Electroluminescence, photoluminescence
Condition control: Temperature Humidity Sample size	 0–100 °C, ± 0.1 °C
High voltage application: Sheet sample (thickness 2 mm) Cable sample (thickness 3 mm)	 150 kV 550 kV

2.4 System Requirements

A key performance criterion for a PEA system is its resolution. In the case of spatial resolution it is not enough to indicate only the absolute resolution (in µm) because the sample thickness changes between measurements. A more general way to express the resolution is to use relative resolution η as given in Equation (2.4). It is determined by the relation between the duration of the pulse voltage ΔT_p and the duration of the acoustic wave in the sample T:

$$\eta = \frac{\Delta T_\mathrm{p}}{T} = \frac{\Delta T_\mathrm{p}}{d/u_\mathrm{sa}}. \tag{2.4}$$

As can be seen from Equation 2.3, in addition to the space charges the measured signal consists of the response of the electrode surface charges. The relation between the signals induced by these two types of charges has influence on the system resolution. In a closed circuit the sum of the charges, which is indicated by the area of the signal pulse, must be zero. Therefore if the surface charge signal is very large compared to the space charge signal, it is difficult to observe the space charge. In the opposite case both the signals widen out again making the distinction between the signals more difficult. This effect is more closely studied in a report by International Council on Large Electric Systems (CIGRE), which also discusses several details of a PEA measurement setup [26]. It has been concluded that setting the relative resolution to 2–5 % gives good outcome. This sets the requirement for the pulse width according to Equation 2.4. Different pulse widths for a range of sample thicknesses at 2 % and 5 % resolutions are compiled in Table 4 for selecting the optimal pulse width. Based on the calculated data, a pulse width of 10 ns was selected for the system as an optimal compromise within the range of 0.2–1 mm sample thicknesses. The amplitude of the pulse is also an important factor determining the signal quality. If the pulse is not strong enough, the acoustic signal is also weak and the measurement becomes more affected by noise. The properties of the pulse voltage are investigated closer in Chapter 3.

Table 4. Calculated pulse widths for different sample thicknesses and target resolutions.

Sample thickness (mm)	Pulse width (ns)	
	Resolution 2 %	Resolution 5 %
0.1	1.0	2.6
0.2	2.1	5.1
0.3	3.1	7.7
0.4	4.1	10.3
0.5	5.1	12.8
1	10.3	25.6

Another factor that influences the output signal quality is the acoustic impedance matching between the high voltage electrode and the sample. Impedance mismatch leads to unnecessary reflections and a transmission factor of less than 1, weakening the quality of the detected signal. This can be avoided by adding a layer of semiconducting material with acoustic impedance close to that of the sample material at the top electrode. The material commonly used is a mixture of polyethylene (PE) and carbon black, which is a semiconducting composite with bulk resistivity of 20-50Ω·m. As a general rule, ideal acoustic impedance matching should be striven for at all the material interfaces of the system, but in practice some compromises have to be made. Table 5 shows some properties of the materials that can be used in constructing the PEA system and in the measurement samples. For optimal detection of the acoustic wave, the frequency bandwidths of the piezoelectric transducer and signal amplifier should be as wide as possible, thus minimising the signal distortion when the acoustic wave passes through these components.

Table 5. Material properties of some insulators and conductors as found in literature[1].

Material	Acoustic velocity (m/s)	Acoustic impedance (kg/m^{2}s) x 10^6	Relative dielectric constant ε_r
PVDF (α and β)	2260 (2140)	4.0 (3.8)	13
PMMA	2680 (2740)	6.2 (3.2)	2.6
LDPE	1950	1.8	2.3
PET	2290	2.86	3.4
Aluminum	6420	17.3	-
Brass	4700	40.6	-
Semiconducting material	1950	1.9	-

The PEA system is used to investigate space charges in polymer materials under the influence of a strong DC electric field stress. The required polarisation DC bias voltage depends on the sample thickness. Typically the high electric field stress E is in the range of 2×10^7 to 1×10^8 V/m when testing dielectrics. To observe changes in space charge behaviour in conditions close to the breakdown, sufficiently strong electric field strength needs to be provided according to

$$E > \frac{V_{\mathrm{dc}}}{d}. \tag{2.5}$$

Thus, for samples with thickness between 0.2 mm and 1 mm, a bias voltage supply of 10 kV is sufficient. Based on the above information the exact system requirements for different components can be set and are listed in Table 6.

[1] Values were found in the CIGRE report [26] and in measurement report from MIT [27]. The values in brackets are from the latter reference.

Table 6. Target specifications for the different components of the PEA system.

Specification	Value
Pulse generator Pulse amplitude Pulse width Switching frequency	 800 V 10 ns 100 Hz
DC bias supply	0 – 10 kV
Piezoelectric sensor	BW: 10 kHz–1 GHz
Signal amplifier	BW: 10 kHz–1 GHz Gain: min. 40 dB
Electrode structure dielectric strength	100 kV/mm

The target requirements were set based on general consulting of the previously built PEA systems. The required bandwidths of piezoelectric sensor and signal amplifier are estimates for ideal components that would have minimal influence on the signal propagating through them.

3. ELECTRICAL AND MECHANICAL DESIGN OF A PEA SYSTEM

"A part-per-million is a part-per-million. It's magic. It's the brass ring. It's the holy grail of every measurement artist. It will mesmerize you. It will goad you. It will drive you crazy and, if you're lucky, will reward you. A part-per-million is a part-per-million."

- Jerrold R. Zacharias (1971)

3.1 Overview of the Measurement System

In the previous chapters the principle of the PEA method was described. This chapter introduces the design process of a system that implements the method and fulfils the system requirements as described in Chapter 2. The design relies on previous works on the subject that present some major outlines for setting up a PEA space charge measurement device, such as the CIGRE report [26] and research done by J.M. Alison [28]. This work presents a conventional PEA system for investigating thin polymer sheet samples under DC bias conditions since that is the research focus at ABB China Ltd. The system consists of the following main components:

- Nanosecond high voltage pulse generator
- Adjustable 10 kV DC voltage source to provide DC bias for measurements
- Adjustable 2 kV DC voltage source to provide input for the pulse generator
- Upper electrode module with pulse and DC bias voltage connectors
- Thick aluminum plate as the lower (ground) electrode
- Piezoelectric transducer and measurement signal output line
- Wideband high gain signal amplifier
- High speed digital sampling oscilloscope

Figure 3 shows a system level diagram of the PEA measurement device. High voltage DC source provides a bias voltage for studying the behaviour of space charges under a HV electric field similar to real situation for example in HV transmission cables. In addition, a shielding case for the piezoelectric PVDF transducer and the signal amplifier is used to avoid EMI issues during the measurement. The measurement output signal is

collected for analysis with a digital sampling oscilloscope. A photograph of the complete PEA system is presented in Appendix B.

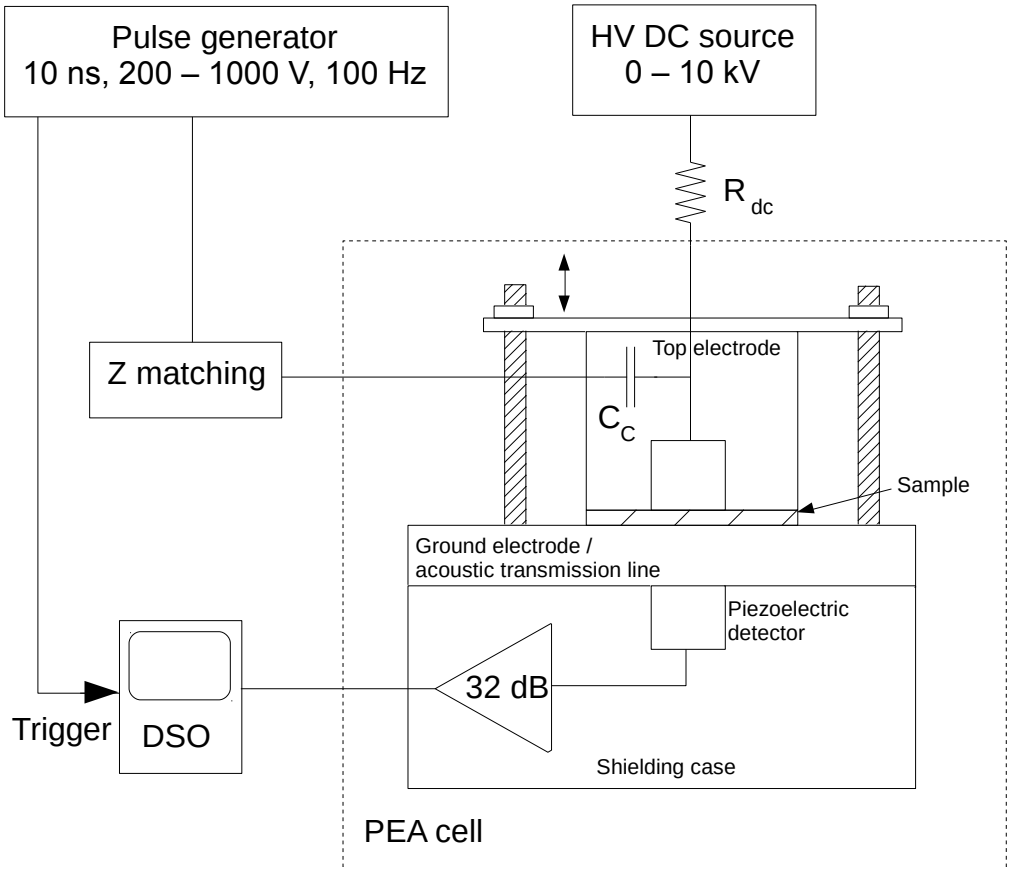

Figure 3. System level block diagram of the PEA measurement system realised in the work.

3.2 High Voltage DC Source

To test the samples in conditions that simulate their real operating environment under high electric field stress, a PEA system uses DC bias voltage applied over the sample. For this purpose, a compact custom-made DC voltage supply was constructed. Figure 4 presents the schematic of the voltage supply. No additional considerations for device cooling were necessary because of the low power consumption in the system.

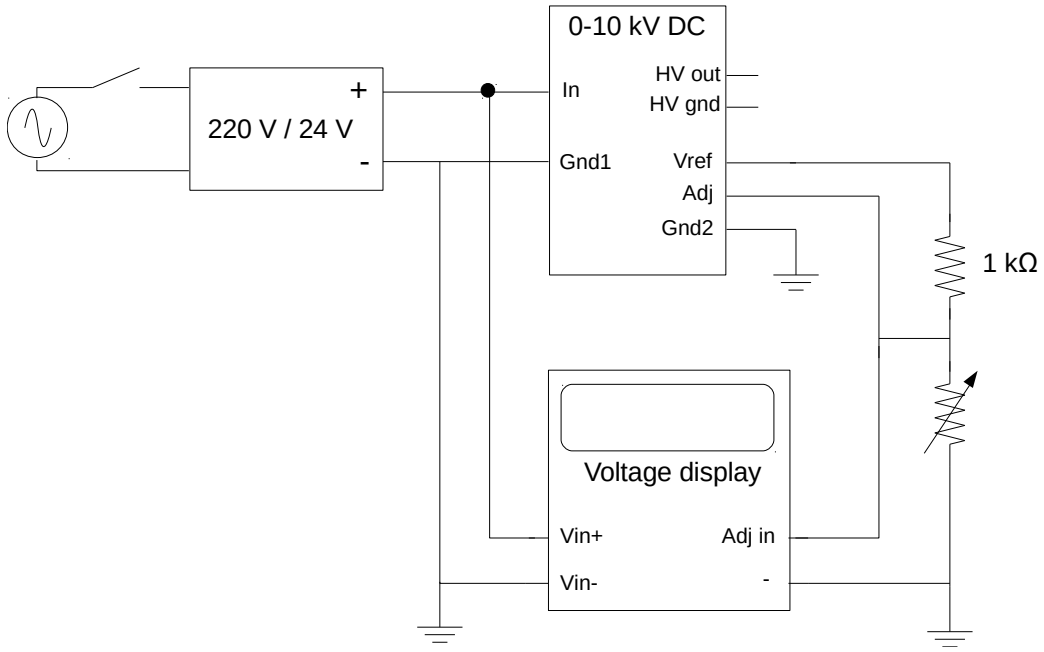

Figure 4. A diagram of the adjustable HVDC supply.

As shown in the system diagram in Figure 3, the HVDC source is connected to the PEA system via a series resistor R_{dc}. This is for two reasons. Firstly, the DC power source, pulse source coupling capacitor and sample are in a configuration that results in voltage division between their equivalent capacitance C_{dc}, C_c and C_s respectively. C_{dc} is estimated to be several mF while C_c is 10 nF. The selection of C_c is explained more closely later on. Viewing the circuit as shown in Figure 3 form the pulse generator side, C_{dc} and C_s appear to be parallel connected. Since C_s is much smaller, usually few tens of pF, this will result in an equivalent circuit where the load capacitance C_L consists mostly of C_{dc}, resulting in most of the pulse voltage v_p being applied to the C_c instead of the sample, according to the equations:

$$v_{sa} = v_p \frac{C_c}{C_c + C_L}, \tag{3.1}$$

$$C_L = C_{dc} + C_s \approx C_{dc}. \tag{3.2}$$

Adding the series resistor eliminates this situation by limiting the current flowing from the pulse source into the direction of the DC power source, allowing it to be applied mostly into the sample instead. Only the current that flows into the sample contributes to the measurement, and the value of the resistance should be accordingly large enough. Its value can be determined from the equation

$$R_{\mathrm{dc}} \gg \frac{1}{2\pi f C_{\mathrm{s}}}, \tag{3.3}$$

where *f* is the main frequency component of the pulse voltage and is determined by the pulse width:

$$f = \frac{1}{2\Delta T_{\mathrm{p}}}. \tag{3.4}$$

Sample capacitance is determined by the material and its thickness *d*:

$$C_{\mathrm{s}} = \varepsilon_0 \varepsilon_{\mathrm{r}} \frac{A}{d}. \tag{3.5}$$

The effective area *A* is determined by the size of the electrode surface. ε_0 is the dielectric constant of vacuum and ε_{r} the dielectric constant of the sample material. The other function of the series resistance is to protect the DC power source and the electrodes in the case of a breakdown in the sample. In such an occurrence, the DC high voltage is applied fully across the series resistor preventing damage to other parts of the circuit. The power dissipating in R_{dc} can be calculated from

$$P = \frac{V_{\mathrm{dc}}^2}{R_{\mathrm{dc}}}. \tag{3.6}$$

The series resistor can now be selected according to Equations (3.3) and (3.6). For calculations a pulse width of 10 ns and sample plate capacitance of 10 pF which is close to the smallest value of C_{s} used in this design are assumed. Giving a multiplier margin of 500, the minimum resistance value for R_{dc} is ca. 150 kΩ. With a maximum voltage of 10 kV in a fault situation, this would lead to unnecessarily large power dissipation in the resistor that would probably destroy any component with low power rating. Therefore, a large 30 MΩ resistor with 5 W power rating was selected.

For DC high voltage output, a custom-made power supply module from Tianjin Dongwen High Voltage Power Supply Co., Ltd. was used. The output current is internally limited to 5 mA. The module requires a DC voltage supply of 24 V to operate. For this purpose, a regular commercial DC converter module with maximum output power of 25 W was implemented in the design. The voltage output can be adjusted by a 10 kΩ potentiometer using an internal voltage division circuit of the module. This was realised by a scale dial connected to resistors of different values for attaining a desired

reference voltage at the adjust-input of the module. The finished HVDC source operates with regular 220 V AC input and can provide output DC voltages of 1, 2, 5, 8 and 10 kV.

3.3 Voltage Pulse Generator

As described in previous chapters, the PEA measurement relies on a fast high-voltage pulse to stimulate space charges for producing a measurable signal. This kind of voltage pulse can be generated in several ways. Since commercial pulse generators are typically very expensive, a simple single purpose generator was designed to provide the high voltage impulse required in the measurement. Regular HV semiconductor switches would seem to be a good choice, but so far their switching speeds are too slow for directly attaining pulse width in the order of few nanoseconds. Another challenge is to reach large enough slew rate *dV*/*dt* to attain an impulse with amplitude of several hundred volts. There is some research being done on a new type of extremely fast power semiconductor switches. Devices that are based on tunnelling-assisted impact ionisation fronts could be used to form voltage pulses with pulse width less than 100 ps, a ramp up to 1 MV/ns and amplitude up to hundreds of kV have been proposed [29] and further developed and experimented [30]. However, so far there are no commercially available products using this novel technology. Some of the more readily available pulse generation methods found in literature include the following:

- Semiconductor switching circuit [31]
- Marx bank pulser with peaking switch and tailcut switch [32]
- Transmission line line pulser [33]

By using a semiconductor switch and fast recovery diode configuration as described in [31], it is possible to gain a neat pulse output. Downside of this solution is that it is relatively complex and requires careful calculation and experimenting of several parameters. Combining a Marx bank generator with two switches as explained in [32], an extremely fast pulse with amplitude of several kV can be attained. However, constructing a Marx bank generator requires large amount of space making the design less suitable for a compact PEA system. Of these methods, transmission line pulsing was found to be the most applicable for its simple, robust and inexpensive design. This work implemented a modified version of Fletcher-type pulse generator introduced in [26].

3.3.1 Line Type Pulse Generator

A Fletcher-type generator relies on a high-voltage switch and coaxial cable for producing a voltage pulse. Figure 5 presents the schematic of a standard Fletcher pulse generator. A high voltage source is connected to a 50 Ω coaxial cable which is also called the pulse generation line T_1. A series resistor R_0 = 1 M Ω is placed between the voltage source and T_1 to limit current in the circuit. When the switch is turned on, the charged cable discharges through the load resistor R, which generates a voltage pulse. In this case the resistor value is equal to the characteristic impedance of the coaxial cable Z_0 to attain impedance matching. The voltage pulse travels along the cable, and upon reaching the right side is completely reflected back towards the matched load because of the large impedance mismatch between R_0 and Z_0. At the load side, the pulse is not reflected because of matched impedance. The voltage amplitude at the load becomes $V_0/2$ due to the voltage division between the ground-connected matching resistor and Z_0. The pulse width ΔT_p depends mainly on the length of pulse generation line *l* and is corresponding to equation

$$\Delta T_{\mathrm{p}} = 2l\frac{\sqrt{\varepsilon_{\mathrm{r}}}}{c}, \tag{3.7}$$

where *c* is the speed of light and ε_r is the relative dielectric constant of the cable.

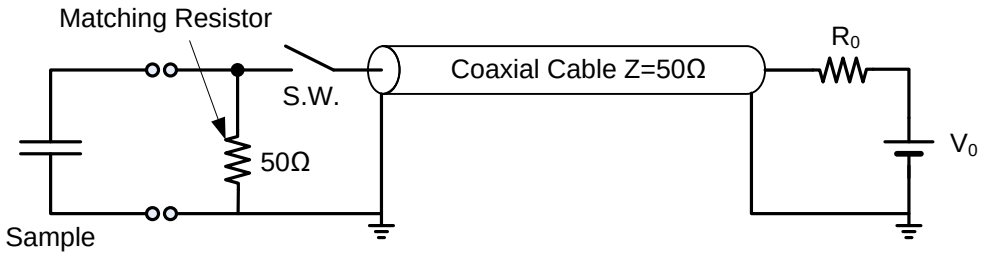

Figure 5. A schematic of Fletcher type transmission line pulse generator [26].

Because of the simultaneous need for an impedance-matched load for reducing voltage pulse ringing and overshoot along with having good voltage pulse efficiency couldn't be satisfactorily met with the aforementioned method, a modified version of the Fletcher type generator was designed. The pulse efficiency η_{eff} is determined by the relation between the pulse voltage peak V_p and the applied DC voltage:

$$\eta_{\mathrm{eff}} = \frac{V_{\mathrm{p}}}{V_{\mathrm{dc}}}. \tag{3.8}$$

To reduce voltage stress on the high voltage switch and the pulse generating line, high pulse efficiency of 50–60 % is a desired feature. A prototype was constructed to adjust the parameters and find out a design for an optimal pulse shape. Figure 6 shows a schematic of this modified pulse generator. Instead of using a 50 Ω matching resistor, a T-attenuator circuit at the end of pulse transmission line T_2 was designed for impedance matching and pulse shaping purposes. T_2 transmits the voltage impulse to the upper electrode of the measurement device. Through experimenting with different lengths of T_1 it was found that at *l* = 90 cm the electromagnetic wave is in a state where its reflected peak is in superposition with the forward propagating peak, resulting in pulse signal amplitude gain of more than 1 at the switch output. This very high efficiency even after counting in dampening in the pulse shaping circuit, the pulse width being close to 10 ns. With smaller values of *l* a faster pulse can be acquired but the efficiency drops radically to around 40 % or less. Because of the modifications to the circuit topology, this practical result wasn't fully predictable from the above mentioned theoretical explanation, although it can still be used as a rough guideline.

The length of T_2 has some influence on the pulse width and efficiency due to attenuation in coaxial cable. Because of the T-attenuator circuit is sufficient for dampening the reflections that inevitably occur at the ends of the transmission line due to more or less imperfect impedance matching, a short T_2 can be used. The length of T_2 used in this application was about 40 cm, having negligible effect on the pulse shape in the transmission line itself.

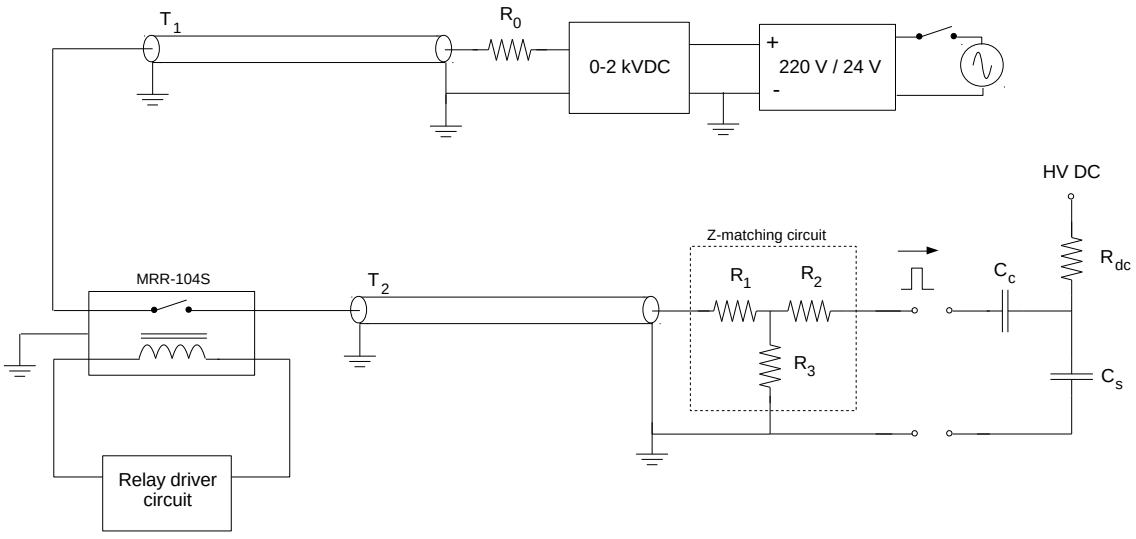

Figure 6. Modified Fletcher type transmission line pulse generator.

For charging the pulse generation line, a high voltage DC power supply with maximum output voltage of 2 kV and low output current was used in the pulse generator. A commercial custom-made power supply from Tianjin Dongwen High Voltage Power Supply Co., Ltd. was selected for use. Its output current is internally limited to 5 mA. Low current with extremely short pulse on-time gives some room for selecting components for the pulse generator because power dissipation is not a major issue. Furthermore, a 1 MΩ / 1 W series resistor R_0 was connected to the voltage output line for additional circuit protection purposes. The DC power supply voltage output is adjustable between 0–2 kV, which is easily achieved by connecting a 10 kΩ potentiometer to the power supply module's internal voltage divider circuit. The power supply requires a DC supply of 24 V to operate. This was realised by using a commercial 220 V / 24 V power converter module. In the final design, 3D-FB coaxial cable was used for both pulse generation and transmission lines. According to the manufacturer's data its dielectric strength is 1.6 kV, which means that the high voltage supply output should be limited to ca. 1.5 kV.

3.3.2 Switching Circuit

There are several options for the high voltage switch, including HV semiconductor switch such as MOSFET, spark gap [31] and mechanical switching relay. The spark gap solution has been found to contain high jitter resulting in significant noise. A spark gap also has a short lifetime compared to relay and semiconductor switches. As mentioned above, so far there are no fast enough semiconductor switches available at the required 1–2 kV range for a single-switch solution. Considering these reasons, a switching relay was used in the pulse generator even though it also has notable switching noise.

A MRR-104S-A wetted reed mercury relay switch rated for 50 W / 2 kV DC and 5 ± 10% V_{cc} was selected. From the component datasheet it can be seen that its maximum switching time is 2.0 ms + 2.5 ms = 4.5 ms, which equals an operating frequency of ca. 220 Hz. To ensure proper operation and longer lifetime, switching frequency f_s = 100 Hz is used. According to the datasheet, the relay's life expectancy is 1×10^9 operations. With the above mentioned operating frequency this means an expected lifetime of roughly 2800 hours for the relay switch. Assuming that the passive components in the circuit suffer no unexpected damage, this is also the estimated lifetime of the pulse generator as a whole. The maximum power dissipating within the switch can be calculated from

$$P_{\max} = f_s \Delta T_p \frac{V_p^2}{R}. \quad (3.9)$$

With switching rate of 100 Hz, 50 Ω load and pulse voltage of 10 ns pulse width and 2 kV peak voltage, the dissipated power is 80 mW which is well within the operational limits of the relay.

A simple control circuit shown in Appendix A was designed for controlling the relay switch. This was realised by a frequency-tuneable oscillator that utilises a LM555 integrated circuit operating in astable mode. An LM7805 voltage regulator was used as low voltage supply for the 555 circuit and the relay. The output signal of the 555 oscillator is amplified by a 2n3904 general purpose NPN transistor, whose output is used to switch the relay and as a trigger signal for oscilloscope when undertaking measurements. A 100 Ω resistor and a 1N4007 diode are connected in parallel over the relay, protecting the circuit from possible kickback currents in the relay.

Since there was plenty of space left to utilise, another 12 V DC supply by LM7812 regulator was implemented on the same circuit board. This 12 V is used to supply a signal amplifier that is described later on. The board is supplied by two low-power transformers that are combined with DF10 diode bridge rectifiers to provide DC voltage input for the voltage regulators. The properties of 78xx series regulators were considered sufficient for the current application. However, there are more precise linear regulators available that also have much lower leakage current. Using one, such as ADP3331 which has low output noise, could possibly reduce noise level in the signal amplifier and thus improve the quality of the measurement to some extent.

3.3.3 Pulse Shaping Circuit

As mentioned above, a separate impedance matching and pulse shaping circuit was designed according to the initial output voltage pulse. The unmatched voltage pulse has a large negative peak and strong tail oscillation (ringing) resulting in poor resolution during space charge measurement. They can be largely eliminated simply by using a long, ca. 30 m, pulse transmission line T_2. The drawback of this solution is reduced efficiency as the pulse amplitude is drastically lowered due to the losses in coaxial cable. Another, more efficient solution is to use a matched T-attenuator at the end of a short transmission line.

In its simplest form, a T-attenuator circuit consists of two series resistors R_1 and R_2 and a ground-connected shunt resistor R_3 between them. By selecting suitable values for the

resistors it is possible to build a circuit with a desired input and output impedance and attenuation value. Selecting 10 Ω for the series resistors and 120 Ω for the shunt resistor gives a circuit that is matched for 50 Ω in both ends and attenuates the passing signal by 3.5 dB. This was used as a basis for the design. However, when connected to the sample through the coupling capacitor, their combined electrical circuit forms a combined load. This is seen by the pulse coming out of the transmission line as a total impedance Z_L and determines the impedance matching between the transmission line and the load. The equivalent circuit shown in Figure 7 is a high-frequency model which takes into account the inductance in the resistor leads and the coupling capacitor leads, together with the DC resistance of the sample sheet.

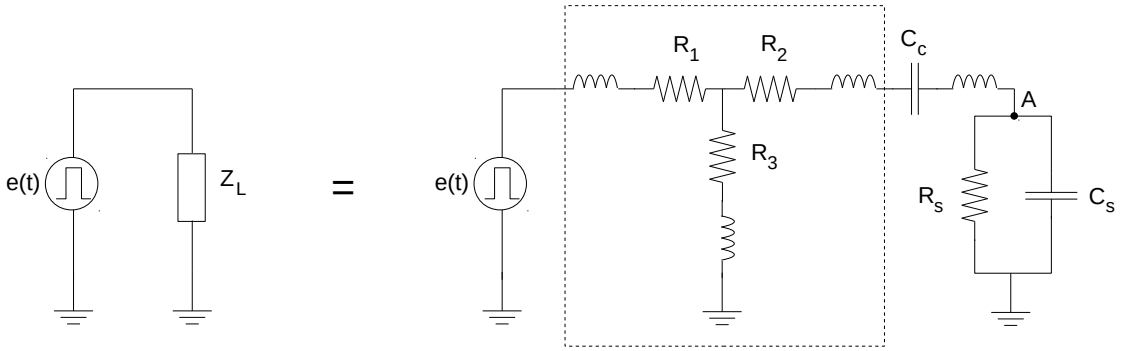

Figure 7. A high-frequency equivalent circuit of the parallel-connected T-attenuator and the capacitive sample.

Optimal values for the resistors in the attenuator circuit had to be found to attain a Z_L value close to 50 Ω for good impedance matching. Equations 3.10–3.14 are used to find the load impedance as seen from the point A in the figure. The impedance was calculated using various sample capacitance and resistor values at frequency of 100 MHz which corresponds to a pulse width of 10 ns. The impedances of the different branches of the circuit are determined as follows:

$$Z_1 = R_1 + \omega L \tag{3.10}$$

$$Z_2 = R_2 + 2\omega L + \frac{1}{\omega C_c} \tag{3.11}$$

$$Z_3 = R_3 + \omega L \tag{3.12}$$

$$Z_s = \frac{R_s}{\omega R_s C_s + 1} \tag{3.13}$$

The impedance at point A is then

$$Z_{\mathrm{A}} = Z_{\mathrm{s}}||[Z_2 + (Z_1||Z_3)] = \frac{Z_{\mathrm{s}}Z_1Z_2Z_3}{Z_{\mathrm{s}}[Z_2(Z_1+Z_3)+Z_1Z_3]+Z_1Z_2Z_3}. \quad (3.14)$$

The DC resistance R_s of the load is large, ca. 1 GΩ. The resistor and capacitor leads were made as short as possible to reduce any parasitic inductance. The inductance values L can be assumed the same and were estimated to be ca. 1 nH. At frequencies below 1 GHz their influence on the impedance remains very small.

According to the equations, R_1 and R_3 have very small influence and the component mainly determining the impedance Z_A is R_2. The actual pulse form and efficiency with input DC voltage of 970 V was observed on an oscilloscope with two different T-attenuator combinations and various samples. Figure 8 shows the calculated pulse efficiency for different sample thicknesses. Through experimenting it was found that a series resistor R_2 of roughly 50–150 Ω gives the best matching in practise. A suitable value for it is needed to attain sufficient dampening of subsequent peaks after the first pulse peak. A larger R_2 will decrease the pulse peak while enabling better pulse form with thicker samples. Even after calculating the attenuation of the pulse shaping circuit, using it gives better pulse efficiency compared to the basic Fletcher type generator because the voltage division can be completely avoided. The pulse shape and peak value are also dependent on the capacitive load C_s, which is determined by the thickness of the sample under measurement. This makes it impossible to completely avoid impedance mismatch. A satisfactory compromise between the ideal pulse form and efficiency with a few different sample thicknesses was achieved by selecting R_2 = 50 Ω. The pulse generator output when connected to a capacitive load is shown in Figure 9.

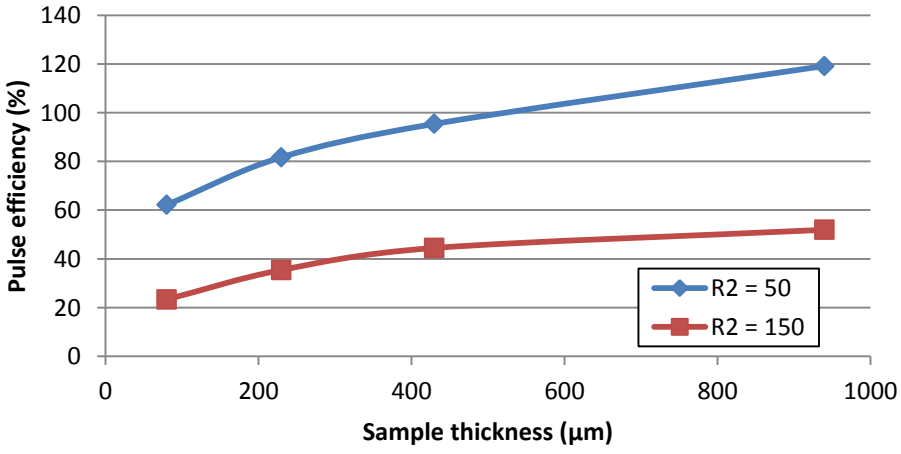

Figure 8. Pulse voltage efficiency as a function of sample thicknesses with two different R_2 values. The sample material is LDPE and input DC voltage 970 V.

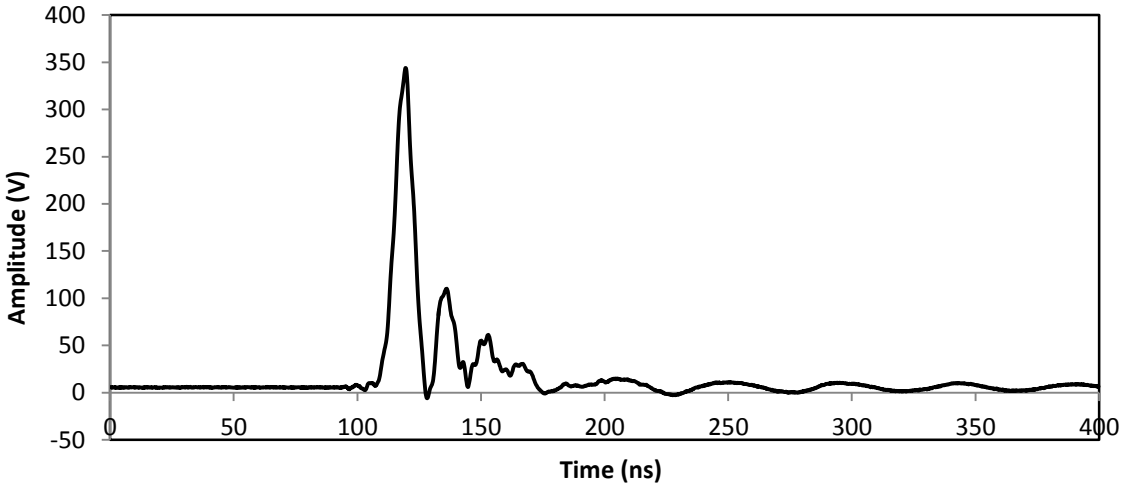

Figure 9. The high voltage pulse when the pulse generator is connected to a 28 pF load capacitance and R_2 = 50 Ω.

The main factor affecting the quality of the critical rising edge of the signal is grounding. Because of the wideband nature of the signal, it is essential to provide wide and well-connected ground paths at all locations to avoid reflections and signal distortion. The same applies to the signal transmission path itself. Good care needs to be taken in soldering the connections and making the transmission path void of any abrupt angles or other discontinuities.

3.3.4 Device Casing

The pulse generator was built inside a casing to protect the circuitry from external RF noise as well as physical disturbances. Another important purpose of the casing is to isolate the user from the high voltage circuitry. The design implements separate switches for switching on the voltage supply and the pulse output. Because of low power dissipation, considerations for extra cooling measures were not necessary. The switching relay can work in ambient temperatures up to 60 °C. Even though the casing is sealed, it's not likely that the inside temperature will rise to that point during normal operation. The pulse generator unit can be directly plugged into a common 220–230 V / 50 Hz power socket.

3.4 Electrodes

Two electrodes for applying the pulse voltage over the sample were designed and constructed. The top electrode is required to have connecting points for the HV DC bias voltage and the pulse voltage as well as housing for the pulse coupling capacitor.

The top electrode module was built within an aluminium shell with insulating Polytetrafluoroethylene (PTFE) ring at the bottom part. The Al cell is electrically connected to the ground electrode by a fastening cap that prevents the module from moving during measurement. The main purpose of the insulator ring is to isolate the high voltage electrode from the ground electrode and increase the distance between them, thus reducing the possibility of flashover along the surface of the polymer sample. Surface flashover is defined as breakdown occurring along an insulator [36] and due considerations should be taken care of when designing high voltage applications. PTFE material was selected for the insulator ring because it is easy to process and has good insulating properties.

The electrode itself consists of a brass cylinder of 20 mm diameter at the contact surface and a brass rod for HVDC connection. 20 mm was selected for the electrode diameter because it is a commonly used value in dielectric breakdown tests. A BNC connector was placed at the side of the cell for pulse voltage input. The dimensions were calculated so that the aluminium cell has room for housing the coupling capacitor that was soldered between the BNC connector and the brass cylinder. The capacitor was placed so that its conducting leads are not close to other conducting parts. After assembling the electrode, the inside housing was cast in epoxy to improve the insulation and prevent voltage discharges between the brass electrode and the aluminium shell. Some designs use a thin semiconducting material layer on the bottom of the HV electrode to attain better acoustic impedance between the sample and the electrode, thus reducing noise caused by reflections at the material interface [22]. However, the semiconducting layer is bound to dampen the pulse voltage and reduce the resolution of the measurement, which is why it was originally left out from this design. However, during testing it was found that the omission of the semiconducting layer results in strong oscillations in the output signal reducing the reliability of the measurement. However, acoustic impedance considerations are more crucial when designing the acoustic transducer element, as explained in the following chapter. Figure 10 shows the top electrode structure.

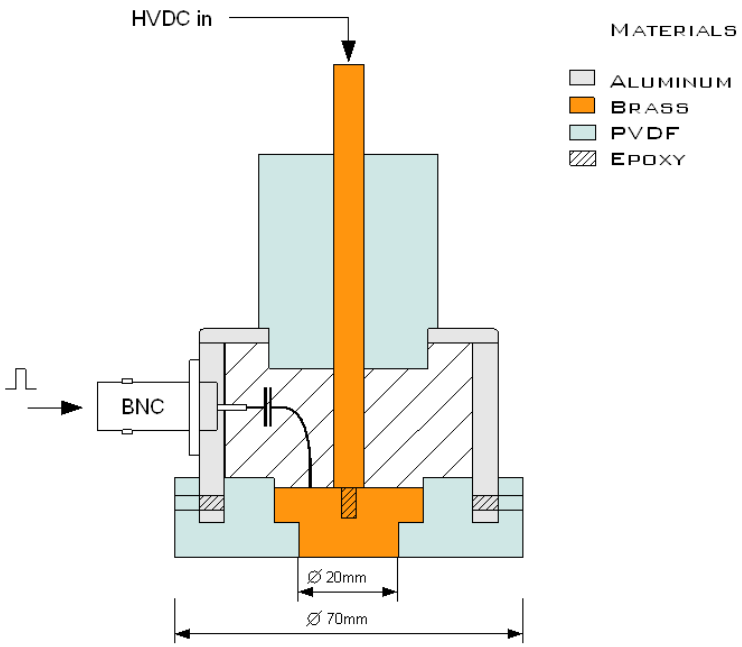

Figure 10. The top electrode was built inside an aluminium cell and insulated with PTFE and epoxy layers.

The coupling capacitor connects pulse voltage to the top electrode while decoupling the pulse generator from the HVDC source, protecting the generator and enabling the DC voltage to be applied to the sample. The pulse voltage is divided between the C_c and the sample capacitance C_s as shown in Equation 3.1. It can be seen that the pulsed voltage across sample $v_{sa}(t)$ is close to the voltage on pulse generator side v_p(t) when C_c is much larger than C_s. The capacitance of a typical sample under measurement is few tens of pF. The ratio for $v_{sa}(t)/v_p(t)$ was calculated for two different sample capacitances using several values of C_c. The graph in Figure 11 shows that selecting a coupling capacitance value of ca. 1 nF enables to 95–99 % of the pulse voltage to be applied over the sample.

Since the maximum DC voltage in the application is 10 kV, the coupling capacitor should be rated for at least this voltage. Regular general purpose ceramic capacitors are well suited for high frequency applications. In this work, a 10 nF, 10 kV ceramic disc capacitor was used. This was found to be sufficient during short periods of testing, even though higher voltage rating is recommended for better long-term reliability of the system.

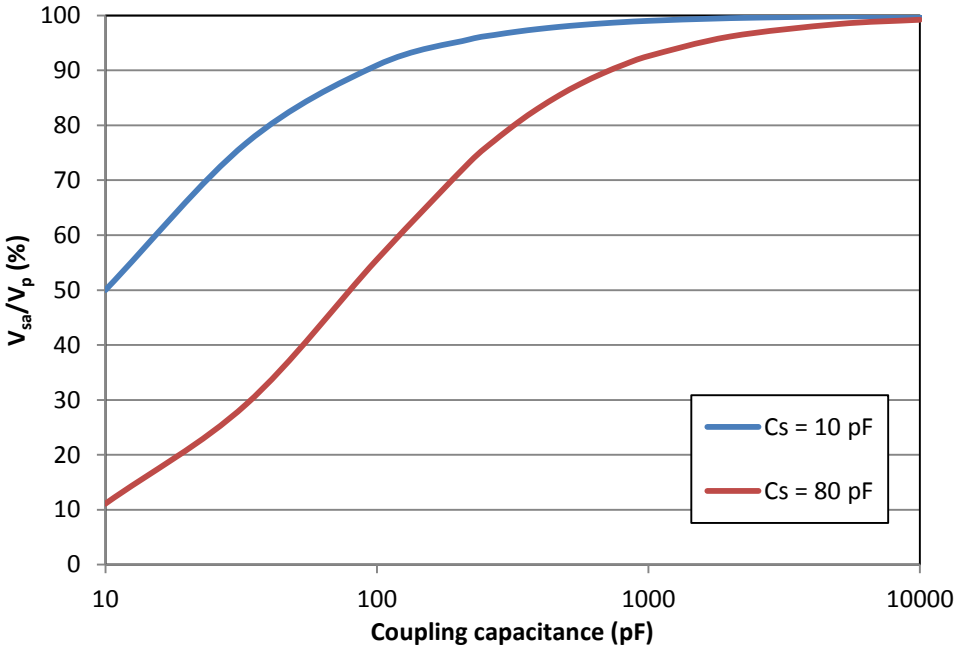

Figure 11. The percentage of pulse voltage applied over two different sample capacitances as a function of the coupling capacitance.

The ground electrode has two main functions: to provide electrical potential reference to the system and to act as a transmission line for the acoustic pressure wave originating from the sample. An aluminium plate with thickness of 20 mm was used as the ground electrode. A thick plate also acts as an acoustic delay line, reducing noise caused by interface reflections and separates the acoustic signal from the electrostatic noise from the voltage pulse switching. To avoid possible dispersion of the acoustic signal arising from structural inconsistencies along the signal path, pure aluminium was used instead of compound material.

3.5 Acoustic Signal Detector

3.5.1 Piezoelectric Transducer

The information concerning the space charge inside a sample is contained in the acoustic wave as described in Chapter 2. A piezoelectric transducer is used to receive the acoustic pulse $p(t)$ and convert it into electrical charge signal $q(t)$. The amplitude of $q(t)$ is proportional to the charge quantity and the sensitivity of the piezoelectric film while the delay indicates the position of the charge[1]. If the transfer function of the

[1] The delay is caused by the different distances of charges from the piezoelectric sensor, which correspond to the spatial locations of said charges.

transducer is written as $h(z = u_b\tau)$, the charge signal can be described as a convolution of $p(t)$ and $h(\tau)$:

$$q(t) = K\frac{u_b}{b}\int_0^\infty h(\tau)p(t-\tau)d\tau. \quad (3.15)$$

In frequency domain the charge signal can be represented as

$$Q(f) = K\frac{u_b\Delta\tau}{b}H(f)P(f), \quad (3.16)$$

where $\Delta\tau$ is the sampling time, u_b is the sound velocity in the transducer and b is the transducer thickness. The transmission coefficient K is determined by the acoustic impedance of the electrode and the transducer material, and is more closely analysed in the following section.

As to the selection of the piezoelectric material to be used in the transducer, the previous studies show that highly polar polyvinylidene fluoride (PVDF-β) has superior properties over the ceramic $LiNbO_3$. The improvements of polymer piezoelectric transducer include high levels of piezo activity, low acoustic impedance, an extremely wide frequency range and a broad dynamic response [35], which contribute to lack of oscillations in the received output signal [36]. The polymeric transducer is a flexible plastic film that can be easily cut and adhered to form transducers according to the user's needs.

The thickness of the transducer is another crucial factor in the measurement resolution alongside the width of the applied voltage pulse. To obtain a high relative spatial resolution, a narrow pulse and thin transducer should be used. In addition, the duration of the acoustic pulse in the transducer should be shorter than the duration of the voltage pulse:

$$\frac{b}{u_b} \leq \Delta T. \quad (3.17)$$

From this equation the transducer thickness can be determined. In PVDF the sound velocity is 2600 m/s, and assuming a voltage pulse width of 10 ns, the thickness should be chosen based on equation

$$b \leq \Delta T u_b = 10\times10^{-9}\ s \times 2600\frac{m}{s} = 26\ \mu m. \quad (3.18)$$

Considering the above requirements, PiezoTech bi-axially stretched and polarised PVDF piezoelectric film with two thicknesses – 9 and 25 µm – was selected for the transducer. The film has Cr-Au metallisation on both sides and can be directly sandwiched between the electrode surfaces without any adhesive medium. The thinner 9 µm film gives better measurement resolution in accordance to Equation 3.18 but its output signal is weaker compared to the thicker 25 µm film and thus more prone to be affected white noise. A thicker film can be used if improved sensitivity is needed.

3.5.2 Acoustic Impedance Matching

Because of using a thin[1] transducer for signal detection, if the acoustic impedances at the transducer-electrode interfaces are different, there will be reflections[2] due to the mismatch that distort the acoustic pressure wave and thus deteriorate the output signal *v*(t). The reflection process with non-matched and matched back electrode is shown in Figure 12. When an acoustic pulse $p_0(t)$ propagates across the ground electrode-transducer interface, part of it is reflected back. This initial reflection can be avoided only by using a ground electrode material with acoustic impedance close to that of the transducer. However, in practice this is not possible because such materials with also good electrical conducting properties do not exist. The transmission coefficient of the wave propagating through the transducer is

$$K_0 = \frac{2Z_\mathrm{p}}{Z_\mathrm{g}+Z_\mathrm{p}}, \tag{3.19}$$

where Z_p and Z_g are the acoustic impedances of the piezoelectric transducer and the ground electrode respectively. The second reflection occurs at the transducer-back electrode interface when the acoustic wave propagates out of the transducer. This second reflection will cause several subsequent reflections within the transducer as shown in the figure. The transmission coefficient of the acoustic wave propagating from the transducer to the back electrode is

$$K_1 = \frac{2Z_\mathrm{b}}{Z_\mathrm{p}+Z_\mathrm{b}}, \tag{3.20}$$

1 Here thin refers to thickness in the range of tens of µm.

2 Because the transducer is very thin, these reflections travel very short distance and thus will not be attenuated much causing the measurement to become noisier if acoustic impedance matching is not done properly.

where Z_b is the acoustic impedance of the back electrode. The total transmission coefficient is then

$$K = K_0 K_1. \tag{3.21}$$

Here the critical term is K_1 which, by selecting an appropriate material for the back electrode, can be modified to be close to 1, resulting in minimal reflections of the acoustic pulse inside the transducer. In an ideal case, the backing material is same as the piezoelectric transducer.

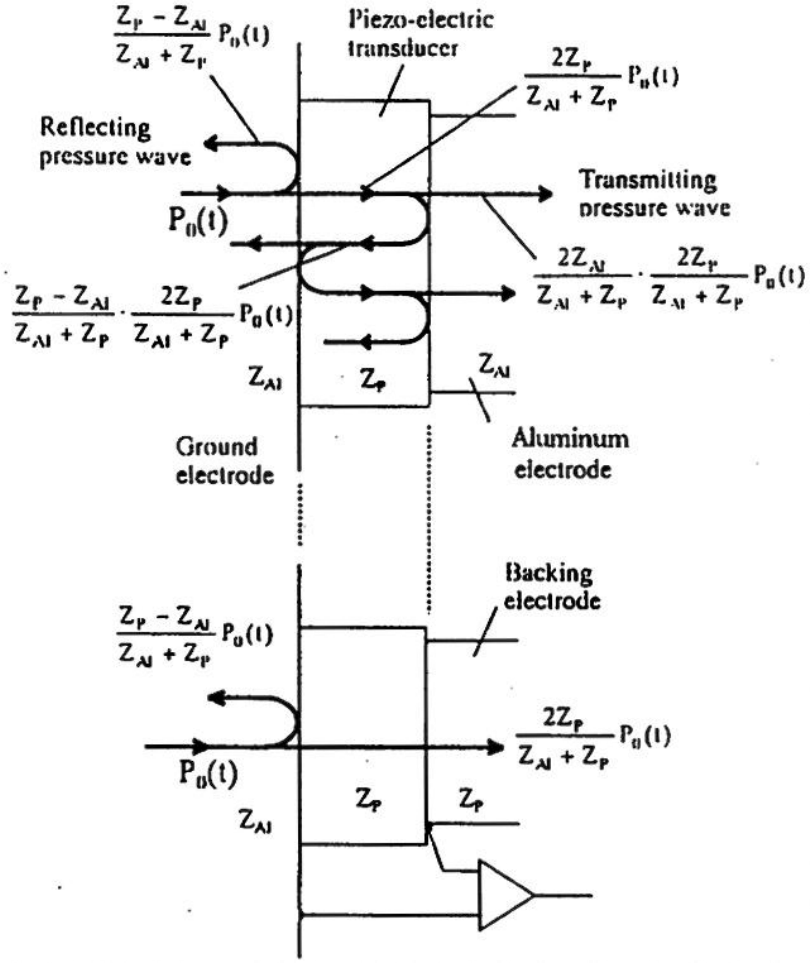

Figure 12. Reflections of acoustic pulse $p_0(t)$ at both surfaces of the transducer when the back electrode is mismatched (top) and matched (bottom) with the transducer [26].

3.5.3 Detector Structure

An acoustic signal detector was constructed according to the principles described above. The detector structure is presented in Figure 13. A PMMA rod with thickness of 17 mm was used as the backing electrode. The rod was covered by a very thin gold plating

using sputtering technique to provide conducting path for the charge signal. The thin gold layer was assumed not to have major influence on the acoustic impedance matching at the transducer-back electrode interface. The thick PMMA also acts as an absorber for the reflections occurring at the back side of the electrode, preventing them from influencing the acoustic signal detection. A thickness of 10 – 20 mm is sufficient to slow down the reflections enough to separate them from the incident pressure wave. On the back side of the electrode, there is a structure consisting of a brass plate, a small hollow brass rod and an SMA connector for signal output. The electrode is placed inside a PTFE tube for electrical insulation. The aluminium shell that contains the whole detector is fastened to the ground electrode by screws. Two silicone rubber rings are placed inside the structure to provide tight contact between the piezoelectric film and the ground electrode.

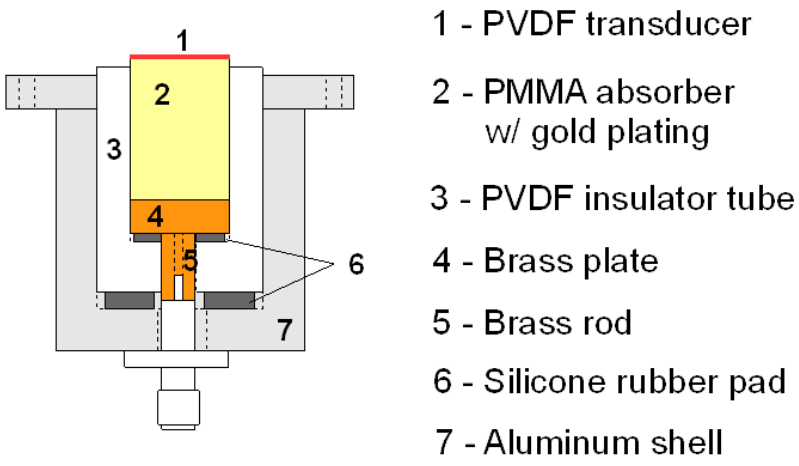

Figure 13. . Cross-section of the cylindrical acoustic signal detector.

The components of the detector were assembled on the back side of the aluminium ground electrode, starting with placing the piezoelectric film on its designated location[1] and subsequently assembling the rest of the components. To provide an optimal path for the acoustic wave propagating from the sample to the piezoelectric transducer, the position of the film should correspond exactly to that of the high voltage electrode.

[1] The position of the piezoelectric film is determined by the location of the high voltage electrode on top of the ground electrode.

3.6 Signal Acquisition System

In a usual case, the output signal of a PVDF piezoelectric transducer is very weak – ca. 10 – 100 µV. Therefore, a signal amplifier is needed to improve the signal to noise ratio of the system. Amplification of ca. 40 dB is sufficient for good signal acquisition. The measurement also contains very wide spectrum of frequencies, and to attain high enough accuracy, the amplifier should have as large a bandwidth as possible. High bandwidth also reduces the low-pass filtering effect of the amplifier circuit, giving better measurement resolution. Among commercial wideband signal amplifiers, a broadband low noise amplifier ABL0300-00-3230 by Wenteq Microwave Corp. was found to meet these requirements. The Wenteq amplifier has a frequency range of 9 kHz to 3 GHz and its nominal gain is 32 dB. To minimise EMI issues originating from external radiation sources, the amplifier was placed inside an aluminium shielding case together with the piezoelectric signal detector.

A Tektronix TDS3012C digital oscilloscope found in the ABB laboratory was use with the PEA system for data acquisition. The oscilloscope has a bandwidth of 100 MHz and sampling rate of 1.25 Gs/s. The oscilloscope has an averaging mode where it displays the waveform as an averaged result of several samplings up to 512 times. This can significantly reduce uncorrelated noise in the signal. Ideally the oscilloscope bandwidth would be greater than 100 MHz which is the equivalent frequency of the 10 ns voltage impulse applied for measurement.

According to the general sampling theorem, a sampling frequency of at least double the measured signal frequency is required to gain reliable results. This requirement is met by the TDS3012C oscilloscope. The acquired signal data can be saved to a USB memory for later processing.

4. SPACE CHARGE MEASUREMENT

To test the functionality of the PEA system, it was used to measure space charge profiles in laboratory. Several low density polyethylene (LDPE) specimens were prepared for measurement samples. First, some reference measurements were conducted at Tsinghua University with their department's own PEA system. Later on a second round of measurements were made at ABB's laboratory. System calibration and signal recovery method are introduced based on the explanation offered by Takada et al. [15]. Detailed analysis of the signal recovery is left outside the scope of this work, but the references provide additional material for the interested reader. The measurement results are presented and analysed in Chapter 5.

4.1 Signal Behaviour in the System

The acoustic pressure waves that contain information of the space charge distribution are converted into charge signals as was described in Chapter 2. The acoustic wave propagating through the sample and the ground electrode is distorted by amplitude attenuation and velocity dispersion. Furthermore, the signal detection circuit consisting of the transducer, signal amplifier and the oscilloscope has limited bandwidth and also causes some distortion on the signal. Of these, the amplifier and oscilloscope can be selected so that their bandwidth is sufficiently large to not have notable influence on the signal quality and can be left outside consideration. Finally, the continuously distributed charges in the sample generate overlapping output signals, which further reduce the system resolution. Especially in the vicinity of the electrodes the signals yielded by volume charges are made less notable by the high amplitude signals generated by the surface charges at the electrode-dielectric interfaces. The effect of these factors can be presented as the system response function $S(f)$ and can be observed in the output signal during calibration. The detected voltage is then determined as was explained by Equation (2.3). Signal processing algorithms can be used in conjunction with calibration measurement to obtain the $S(f)$ by deconvolution and restore the original signal. Various signal recovery techniques such as ones introduced by Tian [37] and Chen [38] have been developed to address the deconvolution problem. In this work, Tian's advanced signal recovery algorithm was used for the numerical processing of the measured signals to examine its effect on signal quality.

4.1.1 System Calibration

The PEA system must be calibrated every time the sample is changed to obtain reliable results. This is because the thickness and intrinsic properties of the sample also affect the system function that must be determined accurately. In addition, the interface properties are bound to change slightly at each assembly of a new sample. The calibration procedure is as follows: first, a DC voltage is applied to the sample to induce surface charges. The voltage is low and short enough to avoid bulk charge formation. Usually a DC voltage of 1 – 2 kV for a few seconds is applied. When a pulse voltage is applied to the sample under this calibration field, the surface charge signal corresponding to $\sigma(0)$ is obtained and can be used as the calibration signal $v_0(t)$. In frequency domain the signal can be written as Equation 4.1, which can be used to obtain the system function. The surface charge can be calculated from Equation 4.2.

$$v_0(f) = \frac{S(f)\sigma(0)}{u_{\mathrm{sa}}\Delta\tau} \tag{4.1}$$

$$\sigma(0) = \varepsilon_0\varepsilon_{\mathrm{r}}\frac{V_{\mathrm{dc}}}{d} \tag{4.2}$$

Inserting $S(f)$ into Equation 2.3 gives Equation 4.3. The left side of the equation shows the bulk charge distribution and the amount of surface charge density at both electrodes. The right side shows the measured voltage signal $V_{\mathrm{out}}(f)$ against the calibrated signal $V_0(f)$. The component $V_{\mathrm{out}}(f)/V_0(f)$ shows the charge distribution in frequency domain, and the charge distribution as a function of position can be extracted by inverse Fourier transform of Equation 4.3.

$$\frac{\sigma(0)}{u_{\mathrm{sa}}\Delta\tau} + R(f) + \frac{\sigma(d)}{u_{\mathrm{sa}}\Delta\tau}exp\left(\frac{-i2\pi fd}{u_{\mathrm{sa}}}\right) = \varepsilon_0\varepsilon_{\mathrm{r}}\frac{V_{\mathrm{dc}}}{d}\frac{1}{u_{\mathrm{sa}}\Delta\tau}\frac{V_{\mathrm{out}}(f)}{V_0(f)}. \tag{4.3}$$

4.2 Measurement Protocol

Some polyethylene terephthalate (PET) and low density polyethylene (LDPE) sample sheets for testing were prepared at ABB research laboratory. Several samples were selected to be used in the testing. Each sample thickness was measured from the centre of the sample. During sample assembly a small amount of silicone oil was applied between the sample and the top and ground electrodes. This is a common technique used in PEA measurements to improve the contact and acoustic impedance matching between the sample and the electrodes. The data obtained from the

calibration phase can also be used to determine the location of the electrodes based on the surface charge peaks.

4.2.1 Reference Measurements

The PEA system was tested at Tsinghua University's facilities. Measurements were conducted with a computer-controlled Tsinghua PEA system, the details of which are presented in Table 7. Because of restrictions at the laboratory, the Tsinghua system couldn't be used to confirm the quality of ABB pulse generator. Afterwards the ABB PEA cell was tested using the Tsinghua system to be able to compare the response of the two systems. Swapping the PEA cells was made easy by similar connectors used in both systems.

Table 7. Comparison of specifications between Tsinghua and ABB PEA systems.

System property	Tsinghua	ABB
Max. pulse voltage	900 V	1000 V
Measurement frequency	1 kHz	100 Hz
Pulse width	6 ns	10 ns
Signal amplifier	60 dB / 1 kHz – 100 MHz	32 dB / 9 kHz – 3 GHz

After calibration, the measurement procedure was as follows: First a polarisation field was applied to the sample for 30 minutes to investigate charge injection in the dielectric. The longer the polarisation time the more visible the bulk charges become in the measurement. This phase is typically referred as "volt on" measurement. After polarisation was finished, the DC voltage was switched off to investigate charge dissipation in the sample. The sample was measured for 10 minutes under this "volt off" state. Samples 1, 2a and 2b were measured using Tsinghua system. Another sample 3 was used to investigate the system response of the ABB PEA system under 2 kV polarisation voltage. The measurement was conducted first without a semiconductor layer at the top electrode and again with a semiconductor added between the top electrode and the sample. The measurements are summarised in Table 8.

Table 8. Samples and their respective measurement conditions for reference measurements at Tsinghua University.

Sample no.	Material	Thickness (um)	Calibration Voltage (kV)	Polarisation field (kV/mm)	Volt on time (min)	Volt off time (min)	PEA cell
1	LDPE	226	2	75	30	10	Tsinghua
2a	LDPE	230	2	75	30	10	Tsinghua
2b	LDPE	150	1.5	100	30	10	Tsinghua
3	LDPE	100	2	-	-	-	ABB

The measurements were observed with LeCroy WaveRunner 6100 digital oscilloscope with a bandwidth of 1 GHz and maximum sampling rate of 2.5 Gs/s. 500 data points were sampled at a time, resulting in sampling time of 200 ns. This is enough to obtain the whole response of the PEA system. The data was stored every 5 seconds from an average of 400 samplings.

4.2.2 System Test Measurements

In the second test round, the ABB PEA system was fully utilised to measure several LDPE samples of varying thickness as presented in Table 9. Because of the lack of CPU control, it was not practical to do large amount of measurements with short intervals. The measurement procedure was conducted manually as follows: First low calibration field strength was applied on the sample as was done previously. Then a polarisation field was applied for 10 minutes at a time. Between each polarisation period (10 minutes), the DC voltage was switched off and the pulse generator was connected to apply the voltage pulse on the sample for obtaining the space charge profile. It was noticed that the coupling capacitor was discharging through the BNC connector after switching off the DC voltage. This was because the capacitance value was relatively large leading to big charge storage inside the capacitor. To avoid any potential damage to the pulse generator and to keep the external charges out of the measurement, the capacitor was fully discharged through a ground-connected resistor every time before connecting the pulse generator. This was repeated several times for each sample to observe the space charge accumulation as a function of time.

Table 9. Samples and their respective measurement conditions for system test measurements at ABB.

Sample no.	Material	Thickness (um)	Calibration voltage (kV)	Polarisation field (kV/mm)	Polarisation time (min)
1	PET	100	1	50.0	10
2	LDPE	80	1	25.0	30
3	LDPE	230	2	21.7	30
4	LDPE	430	2	11.6	30
4	LDPE	430	2	23.4	20
5	LDPE	940	5	10.6	30

The measurement data was collected by a Tektronix TDS3012C digital oscilloscope with bandwidth of 100 MHz and sampling rate of 1.25 Gs/s. The data was averaged from 64 samplings before storing it for later processing.

4.3 Measurement Errors

There are several types of error sources in the space charge measurement. Here a look on the different types of error and a rough estimation of their role in the system is provided.

Random error

Random error is due to white noise in the system. The main source for white noise is thermal fluctuations inside the measurement system. Other possible source is external RF noise disturbance. The former cannot be avoided, but its influence on measurement accuracy is not significant. The latter can be eliminated by good designing a good electrical shielding case for the signal detection parts.

Systematic error

The system calibration parameters can only be determined with a limited accuracy, giving rise to some error in the measurement. Sample thickness was measured with accuracy of ± 5 µm. The HV DC voltage supply output has an accuracy of ca. ± 1 %. Material parameters include the acoustic velocity and vacuum permittivity ε_r, which are based on absolute values found in literature and contain some margin of error.

Errors in signal detection and data acquisition

The space charge is detected with the help of voltage impulse that has a limited width. That inherently limits the measurement resolution which makes it difficult to detect slight changes in the real charge profile. Another factor is slight ringing present in the voltage pulse, which leads to unwanted response in the dielectric. The limited bandwidth of different parts of the signal detection system causes them to function as low-pass filters further reducing the measurement resolution. This causes inaccuracy in determining the sample properties in spatial dimension. Acoustic mismatching in different material

Errors in numerical processing of the signal

Numerical signal recovery techniques can be used to eliminate some of the error sources originating from the physical limits of the system. However, often the algorithms are unable to restore the signal accurately.

5. RESULTS AND DISCUSSION

5.1 Space Charge Formation

The space charge reference profiles were obtained by applying electric stress field to the samples as described in Table 8. For the 230 µm thick sample 2a this corresponds to applying a bias voltage of ca. 17 kV. The raw data was processed by Gaussian filtering. Here the results for sample 2a are presented. Figure 14 shows the charge profile during calibration. The system response is clearly visible as anomalies in the signal as compared to ideal pulse peaks of equal amplitude and width at both electrodes. The acoustic wave experiences attenuation and dispersion while propagating in the sample. This can be observed from the attenuation and widening of the response peak when it arrives to the ground electrode. The charge density data during volt on and volt off phases are presented in Figure 15 and Figure 16 respectively. In the figures the vertical lines denote the location of the electrodes at both sides of the sample.

.

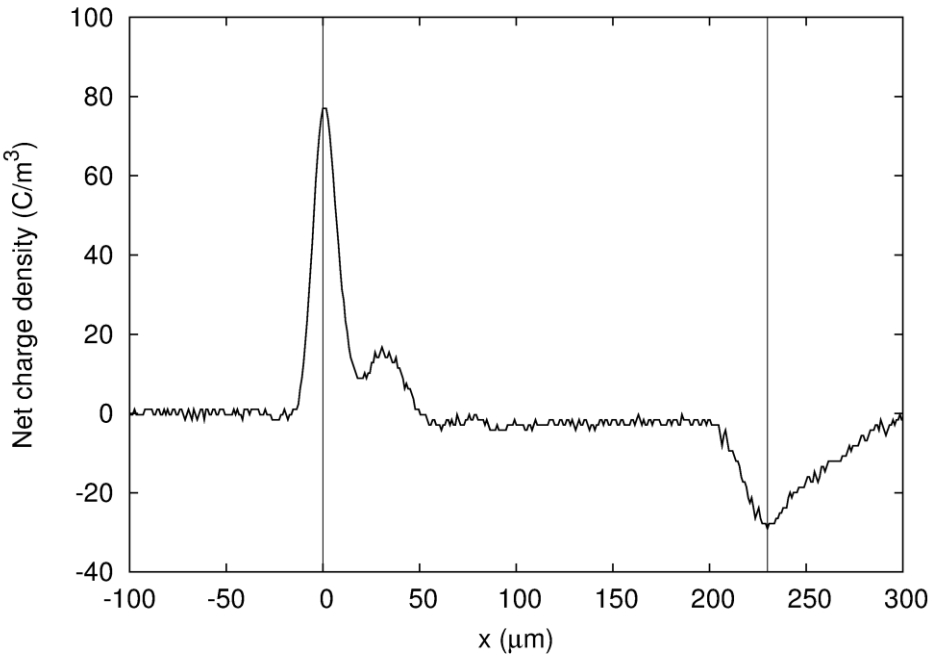

Figure 14. Reference signal obtained by applying 2 kV calibration voltage on 230 µm thick LDPE sample.

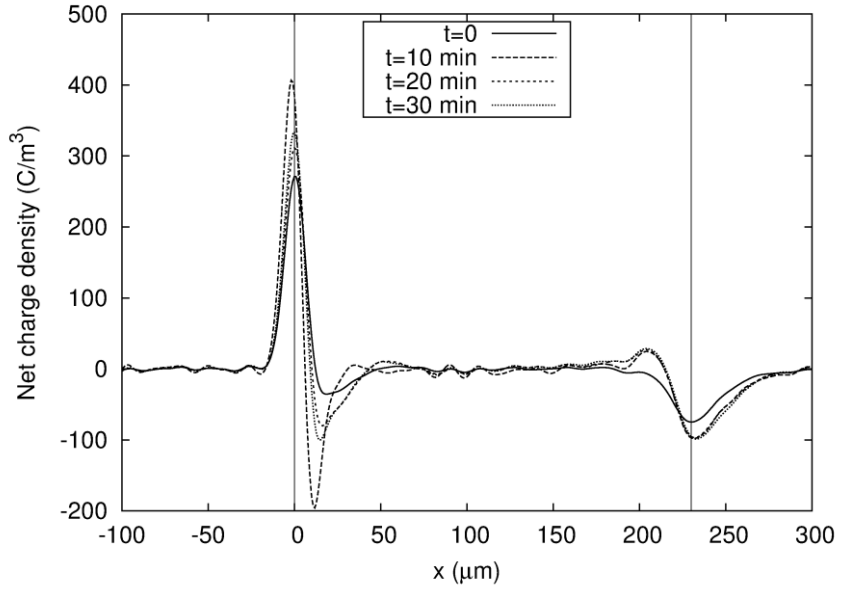

Figure 15. Space charge accumulation in 230 µm thick LDPE sample under 75 kV/mm polarisation field.

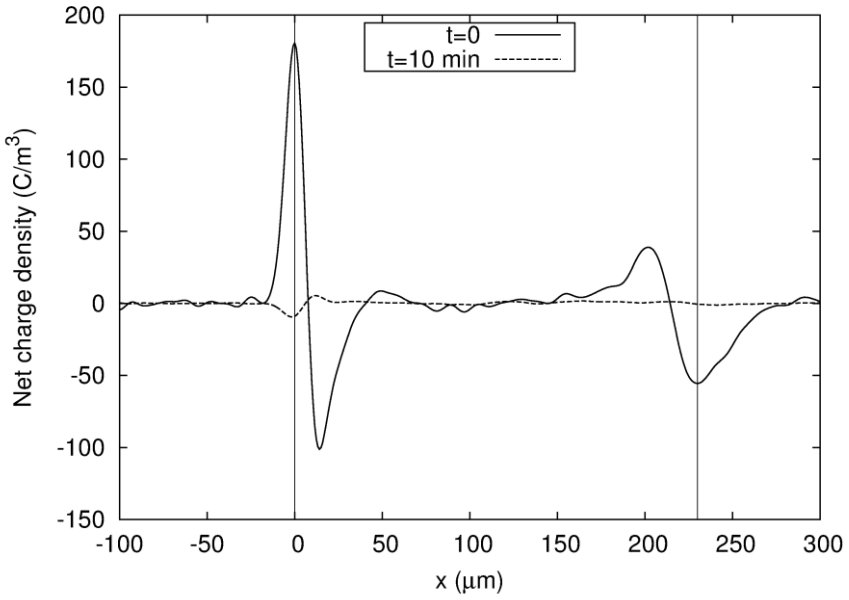

Figure 16. Space charge dissipation in 230 µm thick LDPE sample after switching off polarisation voltage.

Figures 15 and 16 show a typical space charge profile across the thickness of the sample. Very small actual space charge can be observed in the sample bulk. The opposite peaks within the sample bulk next to the surface charge peaks at electrodes occur due to induction of heterocharges. In the volt on -stage, the charges accumulate near the electrodes and slowly migrate into the bulk. This can be seen from the gradual

shift of the net charge from the electrodes into the sample. The total charge density increases steadily with time. By examining the volt off -stage, it can be seen that in 10 minutes the space charge is almost completely dissipated. The charge profile peaks at electrodes are spread out because of the limited resolution of the system, mainly resulting from the limited width of the voltage pulse used to induce the response. Therefore, it cannot be assumed from the figures that there is net charge present outside of the width of the sample. The peaks at electrodes are representations of the actual total charge at an infinitesimally thin surface.

The electric field can be calculated directly the space charge profile according to Poisson's equation:

$$\frac{dE}{dx} = \frac{\rho(x)}{\varepsilon_0 \varepsilon_\mathrm{r}}. \tag{5.1}$$

When the electric field is integrated over the thickness of the sample, its profile can be obtained as shown in Figure 17.

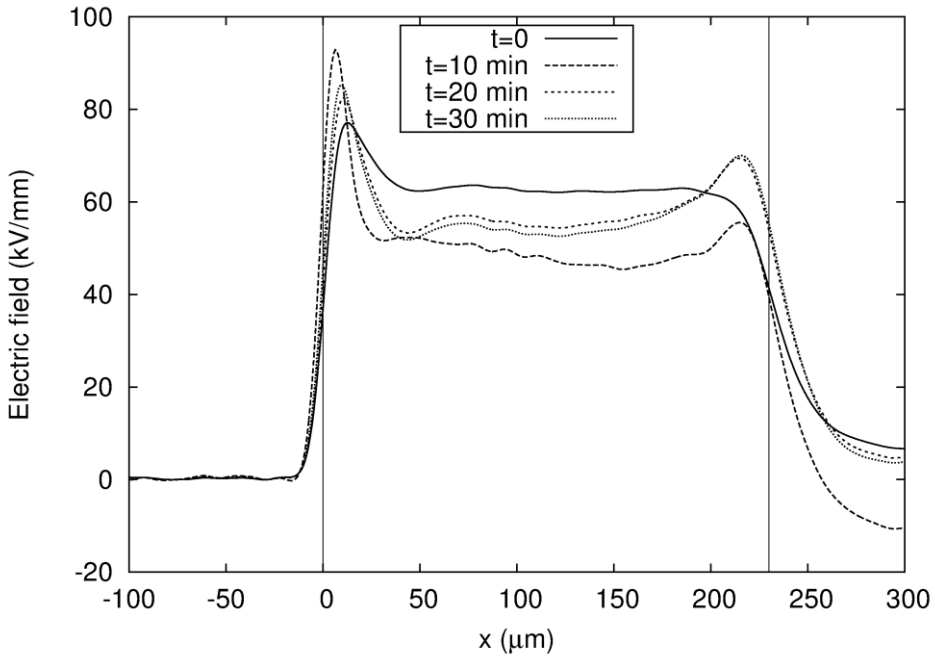

Figure 17. Changes of the electric field profile in 230 µm thick LDPE sample under 75 kV/mm polarisation field.

5.2 System Test Results

Space charge profiles were measured for samples listed in Table 9 by using the PEA system designed in this work. Figure 18 shows the measurement result for sample 3. The half-width of the anode peak in the reference signal (t = 0) can be used to estimate the spatial resolution of the measurement. It is roughly 20 µm. This is in accordance with Equation 2.4 when u_{sa} = 1950 m/s is used for PE material. However, the resolution was found to be too low for reliably measuring samples thinner than 200 µm. The response peaks induced by surface charges move close to each other and make the detecting of any weaker responses between them practically impossible. On the other hand, as sample thickness was increased the output signal became very weak, and couldn't be detected at all when measuring the sample 5. With thickness of 430 µm the signal strength was only ca. 2 mV and increased only when the polarising voltage was doubled to 10 kV.

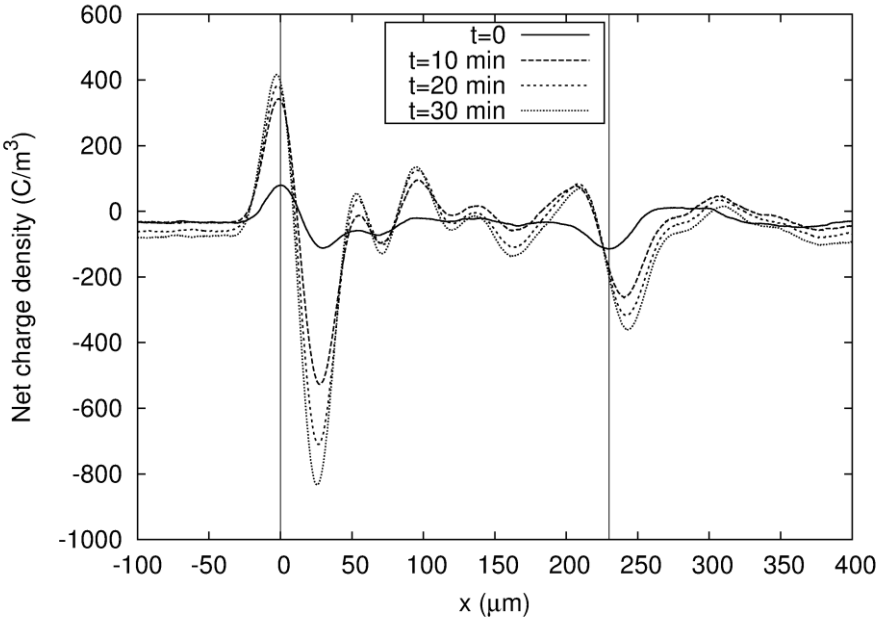

Figure 18. Space charge accumulation in 230 µm thick LDPE sample under 21.7 kV/mm polarisation field.

The influence of averaging to signal quality was investigated by applying the pulse voltage to the sample 3 after polarisation and using different averaging rates to collect the data. Figure 19 shows the oscilloscope screen when using no averaging and averaging with 64 samplings. No averaging results in very noisy output data while averaging rate above 64 was found to have no improving effect. Figure 20 show closer

view the same signals. From Figure 20a it can be seen that the presence of noise will easily cover up any slight changes in the space charge distribution and makes their detection very difficult. By averaging the situation improves notably.

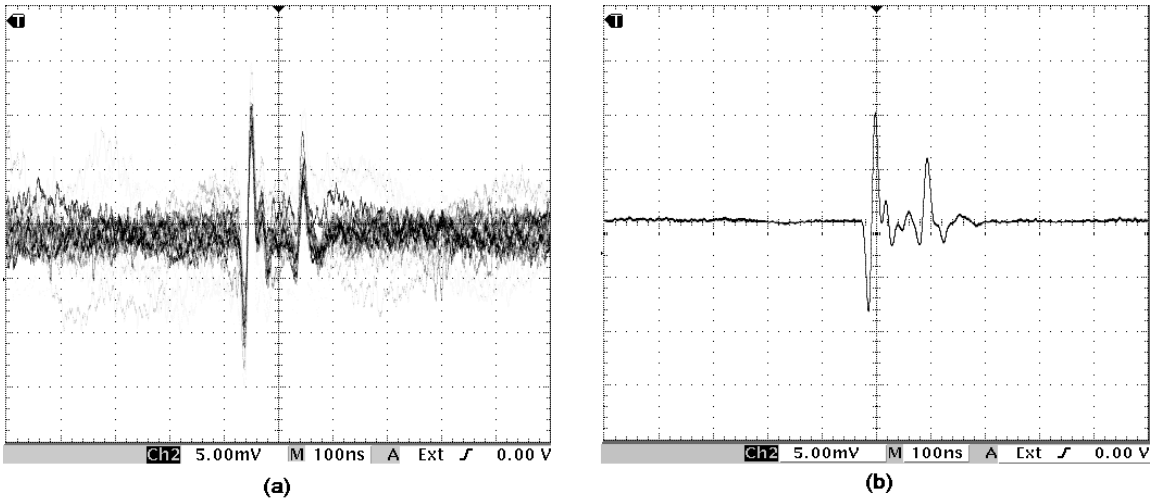

Figure 19. Output signal seen on the oscilloscope screen with a) no averaging and b) averaging with 64 samplings.

(a)

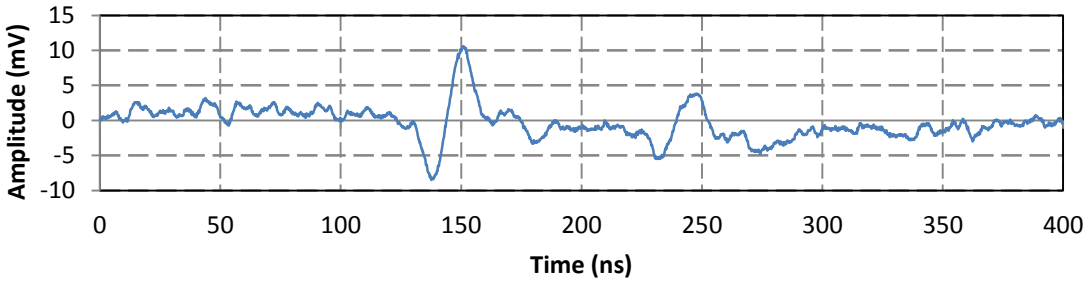

(b)

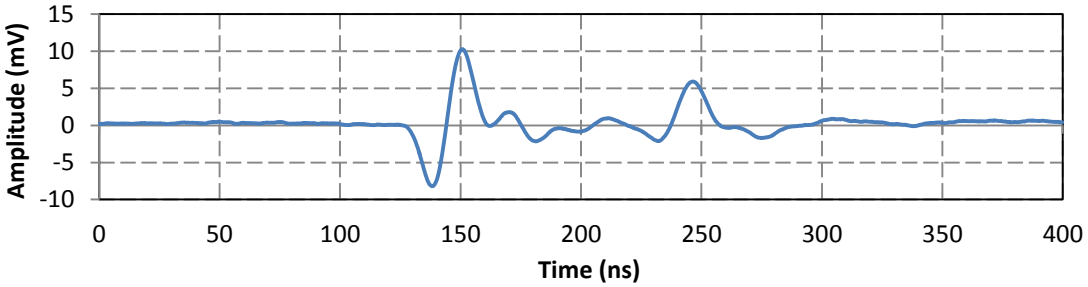

Figure 20. Measured signal with a) no averaging rate and b) averaging rate of 64.

Signal-to-noise ratio of the measurements is determined by the relation between the strength of the signal *S* and average of the noise *n*. Standard deviation formula in Equation 5.2 was used to calculate the average noise. The noise was calculated from

the sampled data excluding a length of 400 ns of data around the actual signal. The number of data points in the noise signal is *N*.

$$\sigma_{\mathrm{n}} = \sqrt{\frac{1}{N-1}\sum_{i=1}^{N}(n_{\mathrm{i}} - \bar{n})^2}. \tag{5.2}$$

The signal strength was determined as the peak value of the output signal. Thus, the signal-to-noise ratio can be calculated from

$$SNR = 20log\left(\frac{\hat{S}}{\sigma_{\mathrm{n}}}\right). \tag{5.3}$$

Table 10 presents the calculated values for σ_{n}, $\hat{S}$ and *SNR*. As with the visual examination of the signal, no notable improvement in the *SNR* was found when averaging rate was increased over 64.

Table 10. Signal-to-noise ratio of the measurement with different averaging rates.

Averaging rate	**Signal peak $\hat{S}$**	**Noise signal σ_{n} (×10^4)**	***SNR* (dB)**
No averaging	0.0106	13.331	41.5
64	0.0103	1.434	85.5

It is possible that the limited bandwidth of the oscilloscope leads to some error in the measurement. If its bandwidth is not clearly larger than the bandwidth of the signal (100 MHz), it functions as a low-pass filter reducing the measurement resolution. The practical effect of the limited bandwidth wasn't investigated further in this work.

During the measurements it was also found out that increasing the pulsed voltage results directly in stronger output signal, which is in accordance with Equation 2.1. The pulse generator was used for five hours in normal room temperature without experiencing any overheating problems despite the closed casing structure.

Signal processing method as introduced in Chapter 4 was applied on the obtained data to examine its effectiveness in recovering the space charge profile. The algorithms are very parameter-sensitive and often times the results are not satisfactory. In actuality, it is very challenging to use the numerical data recovery accurately due to multitude of changing parameters. It is a common practise to observe the space charges directly from the measured data. If the PEA system in question is accurate enough, it can reflect the spatial distribution of charges with acceptable results.

6. CONCLUSION

Space charge characterisation is an important field of electrical insulator research. The PEA method is a common technique for measuring space charges in solid dielectrics. It has been developed to meet research needs in various environments. The objective of this Master's thesis was to design a system to be used as part of ABB (China) Ltd.'s basic research. The design process is documented as a material for later reference.

A PEA lightweight measurement system was designed and constructed for investigating sample plates of 0.2–0.5 mm thickness. The desired system specifications were met with satisfactory results, and the current setup offers a good basis on which to implement further improvements if necessary. The measurement rate of the system is 100 Hz. A DC electric field stress of up to 5×10^7 V/m can be applied on the sample to simulate its operating conditions under strong electric fields. The top electrode has a HV DC connector that can easily be connected also with other DC voltage supplies in case stronger field strengths are required. The spatial resolution of the measurement is 20 µm. When an averaging function of the oscilloscope is used, the *SNR* of the measurement can reach 85.5 dB. The instrument can be used in temperatures from -10 °C to 60 °C. It uses common 220–230 V / 50 Hz AC socket as power supply. The estimated continuous operating life of the device is ca. 2800 h, after which the switching relay of the pulse generator should be replaced.

Future improvements to the system include the following: To attain better measurement resolution, the pulse generator can be improved. Currently its pulse width is ca. 10 ns. Halving that should be quite easy without any major changes, although at the expense of the pulse amplitude, which could lead to weakened output signal of the system. A signal amplifier with larger gain could possibly be used to compensate that. The Piezoelectric film thickness can be changed from 25 µm to 9 µm to improve the spatial resolution. The measuring sensitivity could possibly be improved to some extent by using a PVDF-α instead of PMMA as the back electrode rod material. Another possible addition would be the inclusion of CPU-control for the measurement. The relay control board can be swapped relatively easily for an IC-controlled circuit. This would enable more accurate time resolution in the measurements. The coupling capacitor C_c should be switched to a smaller 1 nF ceramic capacitor instead of the 10 nF currently in use. This would prevent the capacitor from excess charging and discharging during the measurements, which influences the measured signal by injection of additional charges. Another reason for discharging was the insufficient voltage resistance of the BNC

connector. To attain better voltage withstanding capability in the top electrode, a high voltage connector should be used also for the pulse input. To ensure good measurement results, an oscilloscope with bandwidth of more than 100 MHz should be used.

REFERENCES

[1] G. Mazzanti, G.C. Montanari, L.A. Dissado. 2005. Electrical Ageing and Life Models: The Role of Space Charge. *IEEE Trans. Dielectrics and Electrical Insulation*, vol. 12, pp. 876–890.

[2] Y. Zhang, J. Lewiner, C. Alquié. 1996. Evidence of Strong Correlation between Space Charge Buildup and Breakdown in Cable Insulation. *IEEE Trans. Dielectrics and Electrical Insulation*, vol. 3, no. 6, pp. 778–783.

[3] Gorur. G. Raju. 2003. Dielectrics in Electric Fields. pp. 515-516. ISBN: 0-8247-0864-4, Marcel Dekker, Inc.

[4] G. Chen, M.R. Kamaruzzaman. 2007. Impact of Mechanical Deformation on Space Charge in XLPE. *2007 International Conference on Solid Dielectrics, Winchester, UK, July 8-13, 2007*, pp. 510–513.

[5] T. Takada. 1999. Acoustic and Optical Methods for Measuring Electric Charge Distributions in Dielectrics. *IEEE Trans. Dielectrics and Electrical Insulation*, vol. 6, pp. 519–547.

[6] M.A. Noras. 2003. Charge Detection Methods for Dielectrics – Overview. *Trek Application note no. 3005*, TREK, INC. [retrieved in April 24, 2012]. From: http://www.trekinc.com/pdf/3005_Charge_Detection_Methods.pdf.

[7] Y. Li, T. Takada. 1997. Progress in Space Charge Measurement of Solid Insulating Materials in Japan. *IEEE Electrical Insulation Magazine*, vol. 10, no. 5, pp. 16–28.

[8] N. H. Ahmed, N. N. Srinivas. 1997. Review of Space Charge Measurements in Dielectrics. *IEEE Trans. Dielectrics and Electrical Insulation*, vol. 4, no. 5, pp. 644–656.

[9] T. Takada, T. Sakai. 1983. Measurement of Electric Fields at a Dielectric/Electrode Interface Using an Acoustic Transducer Technique. *IEEE Trans. Electrical Insulation*, vol. EI-18, no. 6, pp. 619–628.

[10] T. Takada, T. Maeno, H. Kushibe. 1987. An Electric Stress-Pulse Technique for the Measurement of Charges in a Plastic Plate Irradiated by an Electron Beam. *IEEE Trans. Electrical Insulation*, vol. EI-22, no. 4, pp. 497–501.

[11] K. Fukunaga. 2008. Progress and Prospects in PEA Space Charge Measurement Technique. *IEEE Electrical Insulation Magazine*, vol. 24, no. 3, pp. 26–37.

[12] W. Choo, G. Chen, S.G. Swingler. 2011. Electric Field in Polymeric Cable due to Space Charge Accumulation under DC and Temperature Gradient. *IEEE Trans. Dielectrics and Electrical Insulation*, vol. 18, no. 2, pp. 596–606.

[13] K. Fukunaga. 2004. Innovative PEA Space Charge Measurement Systems for Industrial Applications. *IEEE Electrical Insulation Magazine*, vol. 20, no. 2, pp. 18–26.

[14] K. Fukunaga. 1999. Industrial Applications of Space Charge Measurement in Japan. *IEEE Electrical Insulation Magazine*, vol. 15, no. 5, pp. 6–18.

[15] T. Takada, et al. 1998. Comparison between the PEA Method and the PWP Method for Space Charge Measurement in Solid Dielectrics. *IEEE Trans. Dielectrics and Electrical Insulation*, vol. 5, no. 6, pp. 944–950.

[16] G. Mazzanti, G.C. Montanari, J.M. Alison. 2003. A Space-Charge Based Method for the Estimation of Apparent Mobility and Trap Depth as Markers for Insulation Degradation – Theoretical Basis and Experimental Validation. *IEEE Trans. Dielectrics and Electrical Insulation*, vol. 10, no. 2, pp. 187–197.

[17] M. Fukuma, et al. 2004. High Repetition Rate PEA System for In-situ Space Charge Measurement During Breakdown Tests. *IEEE Trans. Dielectrics and Electrical Insulation*, vol. 11, no. 1, pp. 155–159.

[18] T. Maeno, K. Fukunaga. 1996. High-resolution PEA Charge Distribution Measurement System. *IEEE Trans. Dielectrics and Electrical Insulation*, vol. 3, no. 6, pp. 754–757.

[19] K. Matsui, et al. 2006. High-Sensitivity PEA System with Dual-Polarity Pulse Generator. *Institute of Electrical Engineers of Japan*, vol. 126, no. 3, pp. 178–184. (In Japanese, English version retrieved in April 26, 2012 from: http://onlinelibrary.wiley.com/doi/10.1002/eej.20496/pdf)

[20] T. Maeno. 2001. Three-dimensional PEA Charge Measurement System. *IEEE Trans. Dielectric and Electrical Insulation*, vol. 8, no. 5, pp. 845–848.

[21] T. Maeno, K. Fukunaga. 2004. Open-PEA system for Space Charge Measurement in Dielectrics under Irradiation. *International Conference on Solid Dielectrics, Toulouse, France, July 5–9*.

[22] J.C. Fothergill, et al. 2000. Advanced Pulsed Electro-acoustic System for Space Charge Measurement. *Eighth International Conference on Dielectric Materials, Measurements and Applications, Conference Publication no. 473*, pp. 352–356.

[23] W.S. Lau, G. Chen. 2006. Simultaneous Space Charge and Conduction Current Measurements in Solid Dielectrics under High DC Electric Field. *International Conference on Condition Monitoring and Diagnosis, Changwon Korea, April 2–5.*

[24] T. Muronaka, et al. 1996. Measurement of Space Charge Distribution in XLPE Cable using PEA system with Flat Electrode. *1996 IEEE Annual Report of the Conference on Electrical Insulation and Dielectric Phenomena*, vol. 1, pp. 266–269.

[25] T. Maeno, K. Fukunaga. 2002. Portable Space Charge Measurement System for Space Environment Monitoring. *2002 IEEE Annual Report of the Conference on Electrical Insulation and Dielectric Phenomena*, vol. 1, pp. 853–855.

[26] T. Takada, et.al. 2006. Space Charge Measurement in Dielectrics and Insulating Materials. *CIGRE Task Force D1.12.01-288*. pp. 1–29.

[27] P.E. Bloomfield, W.J. Lo, P.A. Lewin. 2000. Experimental Study of the Acoustical Properties of Polymers Utilized to Construct PVDF Ultrasonic Transducers and the Acousto-Electric Properties of PVDF and P(VDF/TrFE) Films. *IEEE Trans. Ultrasonics, Ferroelectrics and Frequency Control*, vol. 47, no. 6, p.1398.

[28] J.M. Alison. A High Field Pulsed Electro-Acoustic Apparatus for Space Charge and External Circuit Current Measurement Within Solid Insulators. *Measurement Science and Technology*, vol. 9, pp. 1737–1750.

[29] P. Rodin, et.al. 2002. A Novel Type of Power Picosecond Semiconductor Switches Based on Tunneling-assisted Impact Ionization Fronts. *Power Modulator Symposium, 2002 and 2002 High-Voltage Workshop. Conference Record of the Twenty-Fifth International*, *June 30–July 3,* pp. 445–448.

[30] S. Rukin, et.al. 2009. High-Power Picosecond Current Switching by Silicon Diode Using Tunneling-Assisted Impact Ionization Front. *IEEE Pulsed Power Conference 2009*, *Washington DC, US, June 28–July 2,* pp. 287–291.

[31] A. Kuthi, et.al. 2005. Nanosecond Pulse Generator Using Fast Recovery Diodes for Cell Electromanipulation. *IEEE Trans. Plasma Science*, vol. 33, pp. 1192–1197.

[32] J.T. Camp, S. Xiao, K.H. Schoenbach. 2008. Development of a High Voltage, 150 ps Pulse Generator for Biological Applications. *IEEE International Power Modulators and High Voltage Conference*, *Proceedings of the 2008,* pp. 338–341.

[33] L. Liang, et.al. 2003. Development of Compact Nanosecond Pulsed High Voltage Generator. *High Voltage Engineering (Gaodianya Jishu)*, vol. 29, pp. 42–45. (In Chinese, with abstract in English).

[34] J.T. Krile, et.al. 2005. DC and Pulsed Dielectric Surface Flashover at Atmospheric Pressure. *IEEE Trans. Plasma Science*, vol. 33, pp. 1149–1154.

[35] E. Motyl. 2001. Comparison Between Step and Pulsed Electroacoustic Techniques Using Both PVDF and LiNbO3 Transducers. *Journal of Electrostatics*, vol. 51–52, pp. 530–537.

[36] Y. Li, M. Yasuda, T. Takada. 1994. Pulsed Electroacoustic Method for Measurement of Charge Accumulation in Solid Dielectrics. *IEEE Trans. Dielectrics and Electrical Insulation*, vol. 1, pp. 188–195.

[37] J.H. Tian, et al. 2009. An Improved Technique for the Space Charge Distribution Recovery Based on the Profiles Measured by the Pulsed Electro-acoustic Method. *Proceedings of the Chinese Society for Electrical* Engineering, vol. 29, pp. 1–6. (In Chinese, with abstract in English).

[38] G. Chen, Y.L. Chong, M. Fu. 2006. A Novel Calibration Method in the Presence of Space Charge in Dielectric Materials Using the Pulsed Electroacoustic Technique. *8th International Conference on Properties and Applications of Dielectric Materials, Bali, Indonesia, June 26–30,* pp. 289–292.

Appendix A. Control Circuit Board of the Pulse Generator

The pulse generator's switching relay (MRR-104S) is controlled by a simple 555 oscillator, which can be seen in the bottom right corner of Figure AA.1. The 555 oscillator was selected because the electric circuit is very simple requiring small amount of space on the circuit board. The oscillator outputs a square wave with frequency that is tuned to 100 Hz by a 10 kΩ potentiometer R_2. The equation for calculating the oscillation frequency is

$$f = \frac{1.44}{(R_1+2R_2)/C_9} \tag{A.1}$$

Based on the desired frequency of 100 Hz, the other component values were selected as R_1 = 10 kΩ and C_9 = 0.47 µF. The frequency is somewhat instable but in this application there is no need for precise switching frequency. The output current of the LM555 circuit is 200 mA, which in itself is enough to drive the relay. However, a 2n3904 NPN-transistor was used to ensure sufficient drive current.

The 5 V and 12 V voltage supplies were realised with a combination of low-power transformers, DF10 rectifier bridges and voltage regulator chips. The diodes used in the circuit are regular 1N4148 low voltage diodes.

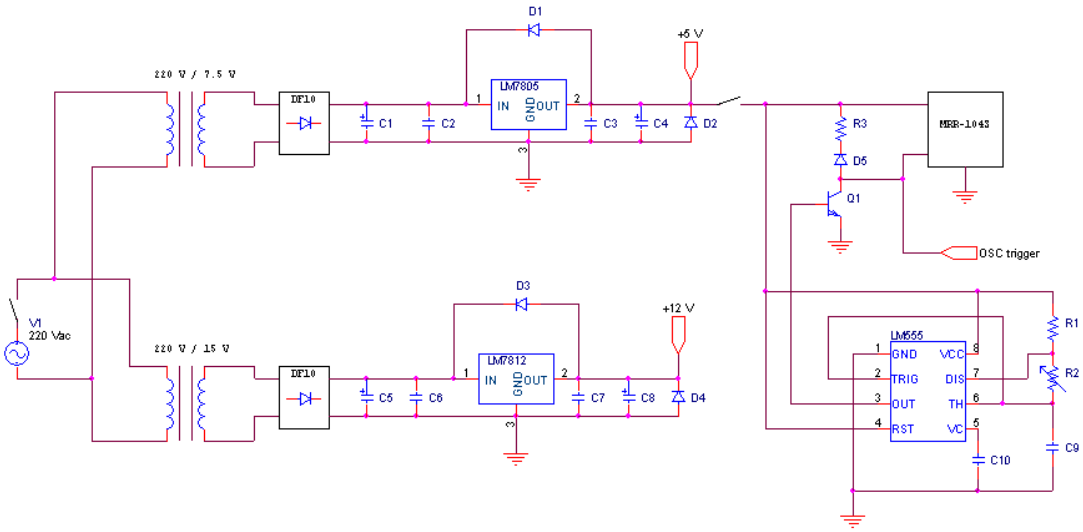

Figure AA.1. Control circuit board containing the relay driver and 5 V and 12 V DC voltage supplies.

.

Appendix B. Photograph of the PEA System

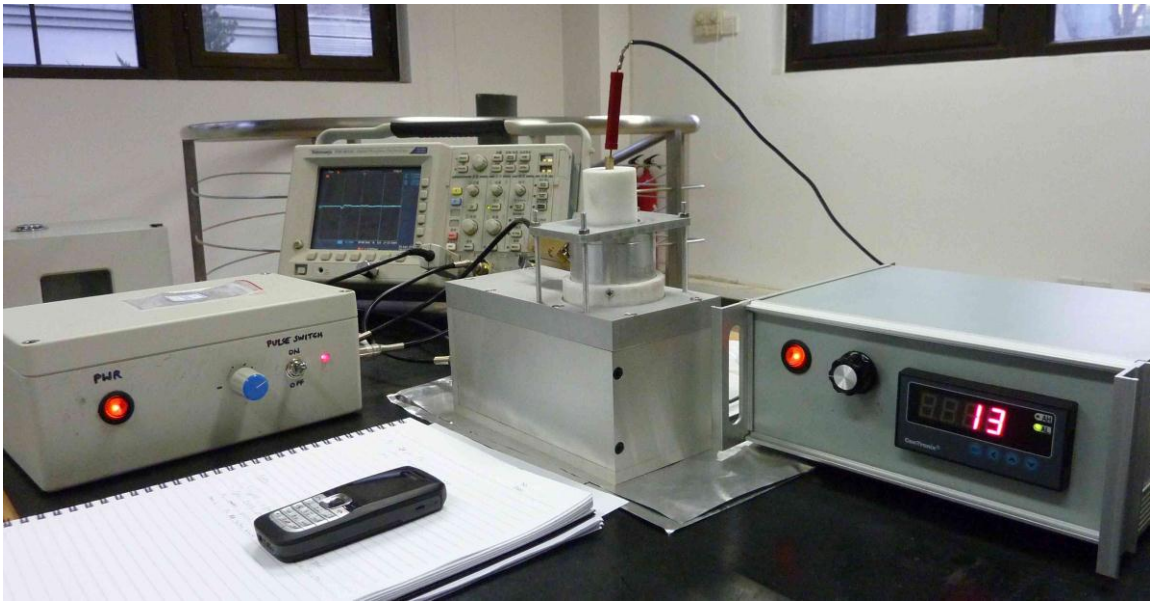

Figure AB.1. The components of the PEA measurement system, from left to right: pulse generator, oscilloscope, PEA cell and HV DC source.